Int. J. Solids Structures Vol. 30, No. 14, pp. 1865–1890, 1993
Printed in Great Britain

0020–7683/93 $6.00+ .00
© 1993 Pergamon Press Ltd

ELASTOPLASTIC CONSTITUTIVE RELATIONS FOR FIBER-REINFORCED SOLIDS

G. DEBOTTON and P. PONTE CASTAÑEDA
Department of Mechanical Engineering and Applied Mechanics, University of Pennsylvania, 220 Towne Building, 220 S 33rd Street, Philadelphia, PA 19104, U.S.A.

(*Received* 12 *August* 1992; *in revised form* 21 *December* 1992)

Abstract—In this paper, we make use of a procedure for estimating the effective properties of nonlinear composite materials, proposed recently by Ponte Castañeda (1991, *J. Mech. Phys. Solids* **39**, 45–71), to study the effective constitutive behavior of ductile, fiber-reinforced composites. Both estimates and rigorous bounds are obtained for the effective energy functions of multiple-phase, fiber composites with general ductile behaviors (in the context of deformation theory of plasticity) for the isotropic constituent phases. The resulting expressions for the energy functions may be differentiated in a straightforward manner to obtain corresponding estimates for the anisotropic effective stress–strain relations. Explicit calculations are carried out for the case of an aluminum-matrix composite reinforced with boron fibers. The results reveal some interesting features distinguishing the constitutive behavior of ductile-matrix, fiber-reinforced composites from that of linear-elastic, fiber-reinforced composites. One such feature is the strong coupling between the dilatational and distortional modes for the ductile fiber composites. Finally, comparisons are made with available experimental data.

1. INTRODUCTION

Fiber-reinforced composites are commonly used materials, and their mechanical properties have been the subject of extensive investigations. However, most of the work to date has addressed exclusively the *linear*-elastic behavior of these materials; details and references can be found in a report by Hashin (1972) and review articles by Willis (1981, 1982) and Hashin (1983). In this paper, we are concerned with the overall behavior of fiber-reinforced composites in which one or more of the phases undergoes *plastic* deformation. The number of papers dealing with this aspect of the behavior of fiber composites is comparatively small. Next, we give a brief review of some of the relevant contributions.

Among the first contributions, Hill (1964b) extended analogous results for the overall elastic moduli of linear-elastic fiber composites (Hill, 1964a) to obtain corresponding estimates for the incremental moduli of ductile fiber composites (in the context of flow theory of plasticity). An alternative approach using the methods of limit analysis to estimate the overall yield strength of composites [see Drucker (1959)] was applied by Shu and Rosen (1967), Majumdar and McLaughlin (1975) and de Buhan *et al.* (1990) to fiber composites. Micromechanical models involving empirical adjustments were developed by Hashin *et al.* (1974), Dvorak and Bahei-El-Din (1987) and Sun and Chen (1991), among others, to predict the yielding and post-yielding behavior of fiber composites. The predictions of some of these models were tested experimentally by Dvorak *et al.* (1988) on a boron/aluminum system. More recently, Zhao and Weng (1990) developed an approximate procedure, based on the Mori–Tanaka (1973) method, for estimating the effective constitutive relations of composites reinforced by aligned spheroidal inclusions, which include fibers as a special case. On the other hand, Talbot and Willis (1991) provided a rigorous bound for the effective energy functions of ductile fiber-reinforced composites by application of a nonlinear generalization of the Hashin and Shtrikman (1962) variational principles, initiated by Willis (1983) and developed further by Talbot and Willis (1985, 1992). In addition, these authors carried out explicit calculations for the case of incompressible fiber-reinforced composites. Ponte Castañeda (1992) obtained similar bounds and additional estimates of the Hashin-Shtrikman type, as well as bounds of the Beran type, for the effective energy functions of incompressible fiber composites through use of a different variational procedure, proposed by Ponte Castañeda (1991a). Finally, Suquet (1992) and Leblond *et al.* (1993) applied an altogether different method to obtain bounds and estimates, respec-

tively, for the overall energy functions of power-hardening materials weakened by cylindrical voids.

Our aim in this paper is to develop and generalize the results of Ponte Castañeda (1992) for fiber-reinforced composites. The method used is based on a variational principle that enables the expression of the effective energy functions of nonlinear composites in terms of optimization problems involving the effective moduli of appropriate families of linear *comparison* composites. Thus, the variational principle suggests a procedure for generating bounds and estimates for the effective behavior of nonlinear composites from *known* estimates and bounds for linear composites with similar microstructures. The procedure was applied by Ponte Castañeda (1991a,b, 1992) to statistically isotropic composites with *general* isotropic constitutive behaviors for the phases. The specific examples of nonlinear materials reinforced by rigid and linear-elastic inclusions, or weakened by voids, were considered in these references. The procedure may also be applied to anisotropic composites. This has been carried out by deBotton and Ponte Castañeda (1992) for ductile *laminated* composites, and by Ponte Castañeda and deBotton (1992) for special classes of anisotropic composites with *rigid–perfectly plastic* phases. In this work, we continue our study of the behavior of anisotropic nonlinear composites by considering the application of the procedure to transversely isotropic, fiber-reinforced composites with general ductile behavior (including compressibility) for the isotropic phases.

The rest of the paper is arranged as follows. In Section 2, we review the definition of effective properties and recall the variational principle of Ponte Castañeda (1992). Next, in Section 3, we make use of the bounds of Hill (1964a) and Hashin (1965) for linear-elastic fiber composites to generate corresponding bounds and estimates for ductile fiber composites. In Sections 4, 5 and 6, we consider some special classes of fiber-reinforced composites, for which the expressions for the bounds and estimates of Section 3 may be simplified further. Thus, we consider the cases of general multiphase *incompressible* fiber composites, hollow-fiber composites, and two-phase, compressible metal-matrix composites. Finally, in Section 7, we compute the effective stress–strain relations of a specific aluminum-matrix composite, reinforced by linear-elastic boron fibers.

2. EFFECTIVE PROPERTIES AND THEIR VARIATIONAL CHARACTERIZATION

In this section, we briefly review the definition of effective properties and their variational characterization. More general discussions, in the context of the inelastic behavior of composite materials, may be found in the articles of Hill (1967) and Suquet (1985). For our purposes, a composite is a heterogeneous material made up of two or more distinct phases, and characterized by two separate length scales: a macroscopic scale L, and a microscopic scale l, such that $l \ll L$. The macroscopic scale describes the gross size of the specimen and the scale of variation of the applied loading, and the microscopic scale characterizes the size of the typical inhomogeneity in the material. Thus, a composite is microscopically heterogeneous, but macroscopically homogeneous.

We consider a representative specimen of the composite Ω, with boundary $\partial\Omega$. For simplicity, we choose units such that the volume of the specimen is unity. We assume that the constitutive behavior of the distinct phases in the composite is characterized by the deformation theory of plasticity or, equivalently, by nonlinear infinitesimal elasticity. However, we note that the usual *approximate* extensions may be made for composite materials characterized by the flow theory of plasticity [see Budiansky (1959) and Hashin *et al.* (1974)]. Thus, at a point $\mathbf{x} \in \Omega$, the relation between the strain field $\boldsymbol{\varepsilon}(\mathbf{x})$ and the stress field $\boldsymbol{\sigma}(\mathbf{x})$ is given by

$$\boldsymbol{\varepsilon}(\mathbf{x}) = \frac{\partial U(\mathbf{x}, \boldsymbol{\sigma})}{\partial \boldsymbol{\sigma}}, \tag{1}$$

where $U(\mathbf{x},\boldsymbol{\sigma})$ is the local complementary energy-density function of the composite.

Then, following Hill (1963), when the composite is subjected to the uniform traction condition

$$\boldsymbol{\sigma}\mathbf{n} = \bar{\boldsymbol{\sigma}}\mathbf{n}, \ \mathbf{x} \in \partial\Omega, \tag{2}$$

where $\mathbf{n}$ is the outward unit normal to $\partial\Omega$ and $\bar{\boldsymbol{\sigma}}$ is a constant symmetric tensor, its effective behavior may be characterized in terms of the *effective complementary-energy function* $\tilde{U}$, with

$$\bar{\boldsymbol{\varepsilon}} = \frac{\partial \tilde{U}}{\partial \bar{\boldsymbol{\sigma}}}, \tag{3}$$

where $\bar{\boldsymbol{\varepsilon}}$ is the mean value of the strain field. We also recall that, under the boundary condition (2), the mean value of the stress field is precisely $\bar{\boldsymbol{\sigma}}$.

In view of (3), the problem of characterizing the effective behavior of the composite reduces to that of computing its effective complementary energy-density function $\tilde{U}$. This may be accomplished directly by means of the principle of minimum complementary energy, stating that

$$\tilde{U}(\bar{\boldsymbol{\sigma}}) = \min_{\boldsymbol{\sigma} \in S(\bar{\boldsymbol{\sigma}})} \int_{\Omega} U(\mathbf{x}, \boldsymbol{\sigma}) \, dv, \tag{4}$$

where

$$S(\bar{\boldsymbol{\sigma}}) = \{\boldsymbol{\sigma} \mid \nabla \cdot \boldsymbol{\sigma} = 0 \text{ in } \Omega, \quad \text{and} \quad \boldsymbol{\sigma}\mathbf{n} = \bar{\boldsymbol{\sigma}}\mathbf{n} \text{ on } \partial\Omega\} \tag{5}$$

is the set of *statically* admissible stress fields. The variational principle (4) is equivalent to a standard boundary value problem, governed by the equilibrium and the compatibility equations, together with the boundary conditions (2). We note that composite materials may exhibit sharp interfaces across which material properties are discontinuous. Consequently, at these interfaces, the equilibrium and compatibility equations must be interpreted in their weak forms enforcing continuity of the tractions and of the tangential components of the strain tensor, respectively.

In addition to the analytical difficulties associated with the heterogeneity of the problem, difficulties also arise because of the nonlinearity of the problem. Precisely to deal with this later difficulty, a variational procedure was introduced by Ponte Castañeda (1991a, 1992). This procedure is based upon a variational principle that expresses the effective energy function of a given nonlinear composite in terms of an optimization problem involving the effective energy functions of a class of *linear comparison composites*. Consequently, well-known estimates and bounds for the effective energy functions of linear composites may be used to generate corresponding estimates and bounds for the effective energy functions of nonlinear composites. Here, we will make use of this method, together with existing results for linear-elastic fiber composites, to obtain bounds and estimates for the behavior of nonlinear, ductile fiber composites.

We will restrict ourselves to composites where all the individual constituents are isotropic with energy-density functions depending only on the first and second isotropic invariants of the stress tensor. Thus, the local complementary energy function may be expressed in the form

$$U(\mathbf{x}, \boldsymbol{\sigma}) = \psi(\mathbf{x}; \tau_e, \sigma_m), \tag{6}$$

where ψ is a nonnegative function, which is convex in its last two arguments and satisfies the condition $\psi(\mathbf{x}; 0, 0) = 0$ for all $\mathbf{x}$. The precise definitions of the two isotropic invariants, the *mean* (hydrostatic) stress σ_m and the *effective shear* stress τ_e, are given by relations (A2). Additionally, we assume that there exists a function $f(\mathbf{x}, v_e, v_m) = \psi(\mathbf{x}, \tau_e, \sigma_m)$ with $v_e = \tau_e^2$ and $v_m = \sigma_m^2$, such that f is convex in its last two arguments (this is the so-called strong convexity hypothesis). This assumption, implying that the dependence of U on the mag-

nitude of the stress tensor is *stronger than quadratic*, is consistent with the anticipated behavior of elastoplastic materials.

In the remainder of this section, we briefly review the variational principle. For further details, we refer the reader to Ponte Castañeda (1992). First, we note that under the above strong convexity assumption, the energy-density function U admits the representation

$$U(\mathbf{x},\boldsymbol{\sigma}) = \max_{\mu_0,\kappa_0 \geq 0} \{U_0(\mathbf{x},\boldsymbol{\sigma}) - V(\mathbf{x};\mu_0,\kappa_0)\}, \tag{7}$$

where

$$U_0(\mathbf{x},\boldsymbol{\sigma}) = \frac{1}{2\mu_0(\mathbf{x})}\tau_e^2 + \frac{1}{2\kappa_0(\mathbf{x})}\sigma_m^2, \tag{8}$$

corresponds to the local energy-density function of a linear-elastic solid with shear modulus $\mu_0(\mathbf{x})$ and bulk modulus $\kappa_0(\mathbf{x})$, and where

$$V(\mathbf{x};\mu_0,\kappa_0) = \max_{\boldsymbol{\sigma}} \{U_0(\mathbf{x},\boldsymbol{\sigma}) - U(\mathbf{x},\boldsymbol{\sigma})\}. \tag{9}$$

Then, substitution of (7) into (4) yields the variational statement

$$\tilde{U}(\bar{\boldsymbol{\sigma}}) = \max_{\mu_0(\mathbf{x}),\kappa_0(\mathbf{x}) \geq 0} \left\{\tilde{U}_0(\bar{\boldsymbol{\sigma}}) - \int_\Omega V(\mathbf{x};\mu_0(\mathbf{x}),\kappa_0(\mathbf{x}))\,\mathrm{d}x\right\}, \tag{10}$$

where

$$\tilde{U}_0(\bar{\boldsymbol{\sigma}}) = \min_{\boldsymbol{\sigma}\in S(\bar{\boldsymbol{\sigma}})} \int_\Omega U_0(\mathbf{x},\boldsymbol{\sigma})\,\mathrm{d}x, \tag{11}$$

is the effective energy function of the linear comparison composite with local energy-density function U_0, as given by relation (8). We emphasize that, under the strong convexity hypothesis, the variational statement (10) (in terms of the linear comparison composite) is completely equivalent to the classical principle of minimum complementary energy.

Next, we specialize the above variational statement to the case of composites with distinct homogeneous phases. Thus, we consider composites made up of n isotropic phases. Each phase is governed by an arbitrary complementary energy-density function satisfying the strong convexity assumption, with $U^{(r)}(\boldsymbol{\sigma}) = \psi^{(r)}(\tau_e, \sigma_m)$ $(r = 1,\ldots,n)$. Then, the local energy function of the composite may be written:

$$U(\mathbf{x},\boldsymbol{\sigma}) = \sum_{r=1}^{n} \chi^{(r)}(\mathbf{x})U^{(r)}(\boldsymbol{\sigma}), \tag{12}$$

where $\chi^{(r)}$ (equals 1 when $\mathbf{x}$ is in phase r, and 0 otherwise) is the characteristic function of the rth phase. The volume fraction of the rth phase is given by

$$c^{(r)} = \int_\Omega \chi^{(r)}(\mathbf{x})\,\mathrm{d}x. \tag{13}$$

An estimate for the effective energy function of the nonlinear composite may be obtained by restricting the set of arbitrary comparison moduli $\mu_0(\mathbf{x})$ and $\kappa_0(\mathbf{x})$ in (10), to the set of piecewise constant moduli (with a different, but constant, modulus over each phase). Consequently, the variational principle (10) yields a bound for the effective energy function of the nonlinear composite (Ponte Castañeda, 1992), given by

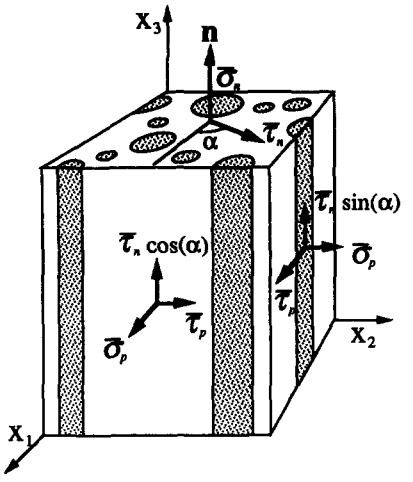

Fig. 1. A two-phase fiber-reinforced composite.

$$\tilde{U}(\bar{\sigma}) \geqslant \max_{\mu_0^{(r)},\kappa_0^{(r)} \geqslant 0} \left\{ \tilde{U}_0(\bar{\sigma}) - \sum_{r=1}^{n} c^{(r)} V^{(r)}(\mu_0^{(r)}, \kappa_0^{(r)}) \right\}, \tag{14}$$

where

$$V^{(r)}(\mu_0^{(r)}, \kappa_0^{(r)}) = \max \{ U_0^{(r)}(\boldsymbol{\sigma}) - U^{(r)}(\boldsymbol{\sigma}) \} \tag{15}$$

and

$$U_0^{(r)}(\boldsymbol{\sigma}) = \frac{1}{2\mu_0^{(r)}} \tau_e^2 + \frac{1}{2\kappa_0^{(r)}} \sigma_m^2. \tag{16}$$

In (14), $\tilde{U}_0$ corresponds to the effective complementary-energy function of a linear composite with the same distribution of phases as the nonlinear composite, i.e.

$$\tilde{U}_0(\bar{\sigma}) = \min_{\sigma \in S(\bar{\sigma})} \int_\Omega \sum_{r=1}^{n} \chi^{(r)}(\mathbf{x}) U_0^{(r)}(\boldsymbol{\sigma}) \, \mathrm{d}x.$$

Thus, each phase is homogeneous and isotropic with shear and bulk moduli $\mu_0^{(r)}$ and $\kappa_0^{(r)}$, respectively. We emphasize that expressions for $\tilde{U}_0$, in the form of bounds and estimates of various types, are available in the literature for several classes of composite materials, including fiber composites. We note that lower bounds for $\tilde{U}_0$ lead through (14) to corresponding lower bounds for $\tilde{U}$, while, on the other hand, upper bounds for $\tilde{U}_0$ lead only to estimates (*not* rigorous bounds) for the corresponding upper bounds for $\tilde{U}$ (we call such estimates *upper estimates*).

3. APPLICATION TO ELASTOPLASTIC FIBER COMPOSITES

In this section, we apply the procedure described in the previous section to obtain bounds and estimates for the effective behavior of elastoplastic fiber composite. Henceforth, the term *fiber composites*, is used to describe the class of n-phase composites with isotropic phases in prescribed volume fractions, and overall transversely isotropic symmetry for the composite. Thus, the microstructure of this class of materials is characterized by a statistically isotropic distribution of the phases in the plane transverse to the symmetry axis **n** (see Fig. 1). In Appendix A, we briefly review some of the properties of transversely isotropic materials, which will be quoted as needed in the developments to follow.

We begin by considering the general case of n-phase fiber composites. Thus, we provide rigorous lower bounds, as well as upper estimates, for the effective energy functions of such composites. In addition, we also provide corresponding expressions for the effective stress–strain relations of such composites. The lower bounds and upper estimates for the effective energy functions of the nonlinear composites are obtained via the procedure described in Section 2 in terms of the corresponding bounds for the effecive energy functions of the class of linear, n-phase, comparison fiber composites.

The constitutive behaviors of the phases of the linear comparison composite may be expressed via the fourth-order elasticity tensors

$$\mathbf{M}_0^{(r)} = \frac{1}{2\mu_0^{(r)}}\mathbf{K} + \frac{1}{2\kappa_0^{(r)}}\mathbf{J}, \tag{17}$$

where the expressions for $\mathbf{K}$ and $\mathbf{J}$, the isotropic projections of the identity tensor, are given by relation (A1). The corresponding energy-density functions $U_0^{(r)}$ are given by (16). Bounds of the Hashin–Shtrikman (1962) type for this class of linear composites were given by Hill (1964a), Hashin (1965) and Walpole (1969).

Following Walpole's representation, we have the following lower bound for the effective energy function of the linear comparison composite, namely,

$$\tilde{U}_0^{(\mathrm{HS}-)}(\bar{\boldsymbol{\sigma}}) = \frac{1}{2}\bar{\sigma}_{ij}(\tilde{M}_0^{(\mathrm{HS}-)})_{ijkl}\bar{\sigma}_{kl}, \tag{18}$$

where

$$\tilde{\mathbf{M}}_0^{(\mathrm{HS}-)}(\mu_0^{(r)}, \kappa_0^{(r)}) = \left[\sum_{r=1}^{n} c^{(r)}[\mathbf{M}_0^{(r)} + \mathbf{M}_0^{*}(\mu_0^{(+)}, \kappa_0^{(+)})]^{-1}\right]^{-1} - \mathbf{M}_0^{*}(\mu_0^{(+)}, \kappa_0^{(+)}). \tag{19}$$

In this relation,

$$\mathbf{M}_0^{*}(\mu, \kappa) = \frac{1}{2\mu}\mathbf{E}^{[1]} + \left(\frac{1}{2\mu} + \frac{1}{\kappa + \frac{1}{3}\mu}\right)\mathbf{E}^{[3]} + \frac{1}{2\mu}\mathbf{E}^{[4]}, \tag{20}$$

where the tensors $\mathbf{E}^{[q]}$ $(q = 1, \ldots, 4)$, the four transversely isotropic projections of the identity tensor, are given by relation (A4), and $\mu_0^{(+)} = \max_r \{\mu_0^{(r)}\}$, $\kappa_0^{(+)} = \max_r \{\kappa_0^{(r)}\}$. Then, upon substitution of (18) into (14), the corresponding lower bound for the effective energy function of the nonlinear fiber composite becomes

$$\tilde{U}^{(\mathrm{HS}-)}(\bar{\boldsymbol{\sigma}}) = \max_{\mu_0^{(r)}, \kappa_0^{(r)} \geqslant 0} \left\{\tilde{U}_0^{(\mathrm{HS}-)}(\bar{\boldsymbol{\sigma}}) - \sum_{r=1}^{n} c^{(r)} V^{(r)}(\mu_0^{(r)}, \kappa_0^{(r)})\right\}, \tag{21}$$

where the functions $V^{(r)}$ are given by relations (15).

Moreover, it is demonstrated in Appendix B that, once the optimization problem (21) is solved, the corresponding estimates for the effective stress–strain relations are given by

$$\bar{\varepsilon}_{ij} = [\tilde{M}_0^{(\mathrm{HS}-)}(\hat{\mu}_0^{(r)}, \hat{\kappa}_0^{(r)})]_{ijkl}\bar{\sigma}_{kl}, \tag{22}$$

where $\hat{\mu}_0^{(r)}$ and $\hat{\kappa}_0^{(r)}$ are the optimized values of the variables $\mu_0^{(r)}$ and $\kappa_0^{(r)}$, respectively. We note that, in spite of its appearance, (22) is *not* a linear relation between the average stress and strain. This is because $\tilde{\mathbf{M}}_0^{(\mathrm{HS}-)}$ depends on the average stress through $\hat{\mu}_0^{(r)}$ and $\hat{\kappa}_0^{(r)}$. We also note that expressions for the stress–strain relations derived from bounds on the effective energy are not guaranteed to be bounds for the effective stress–strain relations of the composite.

Expressions for an upper estimate for $\tilde{U}$, denoted $\tilde{U}^{(\mathrm{HS}+)}$, may be obtained in an

analogous manner. Thus, the upper estimate for the effective energy functions of the nonlinear fiber composites is given by a relation similar to (21) with $\tilde{U}_0^{(\mathrm{HS}-)}$ replaced by

$$\tilde{U}_0^{(\mathrm{HS}+)}(\bar{\boldsymbol{\sigma}}) = \frac{1}{2}\bar{\sigma}_{ij}(\tilde{M}_0^{(\mathrm{HS}+)})_{ijkl}\bar{\sigma}_{kl}. \tag{23}$$

In this expression, $\tilde{\mathbf{M}}_0^{(\mathrm{HS}+)}$ is given by a relation analogous to relation (19), except that $\mu_0^{(+)}$ and $\kappa_0^{(+)}$ are replaced by $\mu_0^{(-)} = \min_r \{\mu_0^{(r)}\}$ and $\kappa_0^{(-)} = \min_r \{\kappa_0^{(r)}\}$, respectively. The associated expressions for the effective stress–strain relations are similar to relations (22), and are given in terms of $\tilde{\mathbf{M}}_0^{(\mathrm{HS}+)}(\hat{\mu}_0^{(r)}, \hat{\kappa}_0^{(r)})$, where $\hat{\mu}_0^{(r)}$ and $\hat{\kappa}_0^{(r)}$ are now the optimized values of the variables $\mu_0^{(r)}$ and $\kappa_0^{(r)}$ arising from the solution of the optimization problem for $\tilde{U}^{(\mathrm{HS}+)}$.

From a practical point of view, the class of two-phase, transversely isotropic fiber-reinforced composites is probably the most important. For this case, Lipton (1991) has shown that the linear bounds (18) and (23) are optimal. The lower bound is attained by a fiber composite made up of a matrix of the stiffer phase weakened by fibers of the softer phase, while the upper bound is attained by a fiber composite made up of a matrix with the more compliant phase reinforced by fibers of the stiffer material. Therefore, the linear bounds $\tilde{U}_0^{(\mathrm{HS}-)}$ and $\tilde{U}_0^{(\mathrm{HS}+)}$ may be regarded as estimates for the effective energy functions of these two types of linear-elastic, fiber-reinforced composites, respectively. It follows from the discussion in Section 2 that $\tilde{U}^{(\mathrm{HS}-)}$ and $\tilde{U}^{(\mathrm{HS}+)}$ may therefore also be regarded as estimates for the effective energy functions of the corresponding classes of nonlinear fiber composites. Thus, we may regard the lower bound (upper estimate) as an estimate for the effective energy function of a nonlinear fiber composite involving fibers (matrices) of the weaker phase, and matrices (fibers) of a stiffer material. In particular, the associated expressions for the stress–strain relations may also be used as estimates for the behaviors of these two types of nonlinear fiber composites with extremal properties. In Sections 6 and 7, we will discuss this possible interpretation of the results in more detail.

To conclude this section, we note that the representations for the lower bound $\tilde{U}^{(\mathrm{HS}-)}$ and the upper estimate $\tilde{U}^{(\mathrm{HS}+)}$ are given in terms of $4n$-dimensional optimization problems. From a computational point of view, obtaining the solutions of these problems is straightforward, especially because the functions $V^{(r)}$ are convex in the optimization variables $\mu_0^{(r)}$ and $\kappa_0^{(r)}$. Nevertheless, in some cases, these representations can be simplified further with the help of the identity given in Appendix C. In the following section, dealing with the special case of incompressible fiber composites, we make use of this approach. In later sections we consider the more complicated case of compressible fiber composites.

4. THE INCOMPRESSIBLE FIBER-REINFORCED COMPOSITES

In this section, we are concerned with fiber composites that are made up of n incompressible phases (and are hence incompressible). Neglecting dependence on the third invariant of the stress, we have that the complementary energy-density functions of the phases depend only on the effective shear stress, i.e.

$$U^{(r)}(\boldsymbol{\sigma}) = \psi^{(r)}(\tau_e). \tag{24}$$

Then, expression (21), together with (15), reduces to the following expression for the lower bound on the effective energy function of the nonlinear fiber composite, namely

$$\tilde{U}^{(\mathrm{HS}-)}(\bar{\boldsymbol{\sigma}}) = \max_{\mu_0^{(r)} \geqslant 0} \min_{\tau_e^{(r)}} \left\{ \tilde{U}_0^{(\mathrm{HS}-)}(\bar{\boldsymbol{\sigma}}) - \sum_{r=1}^{n} c^{(r)} \left[\frac{1}{2\mu_0^{(r)}} (\tau_e^{(r)})^2 - \psi^{(r)}(\tau_e^{(r)}) \right] \right\}. \tag{25}$$

In the above relation, the lower bound for the effective energy function of a linear comparison composite (made up of n incompressible isotropic phases) $\tilde{U}_0^{(\mathrm{HS}-)}$ is given by

relation (18), with $\kappa_0^{(r)} = \infty$ $(r = 1, \ldots, n)$ in expressions (19) and (20) for $\tilde{\mathbf{M}}_0^{(\mathrm{HS}-)}$ and $\mathbf{M}_0^*$, respectively. Then, by means of identity (C2), $\tilde{U}_0^{(\mathrm{HS}-)}$ may be rewritten in the form

$$\tilde{U}_0^{(\mathrm{HS}-)}(\bar{\boldsymbol{\sigma}}) = \frac{1}{2} \min_{\substack{\boldsymbol{\Omega}^{(r)} \\ \boldsymbol{\Omega} = \mathbf{I}}} \left\{ \sum_{r=1}^{n} c^{(r)} \bar{\sigma}_{ij} [\Omega_{klij}^{(r)} [(M_0^{(r)})_{klmn} + (M_0^*(\mu_0^{(+)}))_{klmn}] \Omega_{mnpq}^{(r)} - (M_0^*(\mu_0^{(+)}))_{ijpq}] \bar{\sigma}_{pq} \right\}, \quad (26)$$

where the optimization variables $\boldsymbol{\Omega}^{(r)}$ are subject to the constraint $\sum_{r=1}^{n} c^{(r)} \boldsymbol{\Omega}^{(r)} = \mathbf{I}$, and satisfy the symmetry conditions $\Omega_{ijkl} = \Omega_{jikl} = \Omega_{ijlk}$. In general, expression (26) involves optimization over $36n$ entries of the $\boldsymbol{\Omega}^{(r)}$. However, due to the symmetries of the tensors $\mathbf{M}_0^{(r)}$ and $\mathbf{M}_0^*$, only $6n$ nonzero entries are needed. Thus, the optimization variables may be chosen in the form

$$\boldsymbol{\Omega}^{(r)} = \sum_{q=1}^{6} \omega_q^{(r)} \mathbf{E}^{[q]}, \quad (27)$$

where the definitions of $\mathbf{E}^{[5]}$ and $\mathbf{E}^{[6]}$ are given by (A7) of Appendix A, and where the optimization constraint implies that $\bar{\omega}_q = 1$, $(q = 1, 2, 3, 4)$ and $\bar{\omega}_q = 0$, $(q = 5, 6)$. With this choice for the $\boldsymbol{\Omega}^{(r)}$, $\tilde{U}_0^{(\mathrm{HS}-)}$ can be expressed in terms of the three *imcompressible* transversely isotropic invariants of $\bar{\boldsymbol{\sigma}}$, namely, the deviatoric shear stress $\bar{\tau}_\mathrm{d}$, the transverse shear stress $\bar{\tau}_\mathrm{p}$ and the longitudinal shear stress $\bar{\tau}_\mathrm{n}$ (see Appendix A). Furthermore, $\tilde{U}_0^{(\mathrm{HS}-)}$ depends on these three invariants and the $\omega_q^{(r)}$ $(q = 1, \ldots, 6)$ only through the following $4n$ groups:

$$\bar{\tau}_\mathrm{d}(\omega_1^{(r)} - 2\omega_6^{(r)}), \quad \bar{\tau}_\mathrm{d}(\omega_5^{(r)} - \omega_2^{(r)}), \quad \bar{\tau}_\mathrm{p}\omega_3^{(r)}, \quad \text{and} \quad \bar{\tau}_n\omega_4^{(r)}. \quad (28)$$

However, following a procedure similar to the one described in Appendix B [see the discussion preceding eqns (B8)] to eliminate the optimization constraints, and using the identity $\max_{x,y} \{f(x+y) + g(x)\} = \max_x \{f(x)\} + \max_x \{g(x)\}$, the number of the optimization variables can be further reduced to $2n$ variables. In terms of these variables ($\omega^{(r)}$ and $\eta^{(r)}$), the lower bound for the effective energy function of the linear comparison composite becomes

$$\tilde{U}_0^{(\mathrm{HS}-)}(\bar{\boldsymbol{\sigma}}) = \min_{\substack{\omega^{(r)}, \bar{\omega} = 1 \\ \eta^{(r)}, \bar{\eta} = 1}} \left\{ \sum_{\substack{r=1 \\ r \neq s}}^{n} c^{(r)} \left[\frac{1}{2\mu_0^{(r)}} [(\tau_\mathrm{p}^2 + \tau_\mathrm{n}^2)(\omega^{(r)})^2 + \tau_\mathrm{d}^2 (\eta^{(r)})^2] + \frac{1}{2\mu_0^{(+)}} (\tau_\mathrm{p}^2 + \tau_\mathrm{n}^2)(1 - \omega^{(r)})^2 \right] \right\}. \quad (29)$$

Upon substitution of (29) into (25), we arrive at the following expression for the lower bound for the effective energy function of the nonlinear, incompressible fiber composite $\tilde{U}^{(HS-)}$, namely:

$$\tilde{U}^{(\mathrm{HS}-)}(\bar{\boldsymbol{\sigma}}) = \min_s \min_{\substack{\omega^{(r)}, \bar{\omega} = 1 \\ \eta^{(r)}, \bar{\eta} = 1}} \left\{ \sum_{\substack{r=1 \\ r \neq s}}^{n} c^{(r)} \psi^{(r)}(\tau_\mathrm{e}^{(r)}) + c^{(s)} \psi^{(s)}(\tau_\mathrm{e}^{(s)}) \right\}, \quad (30)$$

where

$$\tau_e^{(r)} = \sqrt{(\bar{\tau}_p^2+\bar{\tau}_n^2)(\omega^{(r)})^2+(\bar{\tau}_d\eta^{(r)})^2}, \quad (r=1,\ldots,n; r\neq s),$$

$$\tau_e^{(s)} = \sqrt{(\bar{\tau}_p^2+\bar{\tau}_n^2)\left[(\omega^{(s)})^2+\sum_{t=1}^{n}\frac{c^{(t)}}{c^{(s)}}(1-\omega^{(t)})^2\right]+(\bar{\tau}_d\eta^{(s)})^2}. \tag{31}$$

Expression (30) was obtained from (25) by interchanging the order of the optimization operations over the variables $\mu_0^{(r)}$ and the $\omega^{(r)}$, $\eta^{(r)}$ variables, respectively. This is allowed by the Saddle Point Theorem (Rockafellar, 1970) since the functions $(-V^{(r)})$ are concave in the variables $\mu_0^{(r)}$, while (29) is convex in the variables $\omega^{(r)}$ and $\eta^{(r)}$. Also, the minimum over S implied by $\mu_0^{(+)}$ in expression (29) has been taken outside in expression (30). In addition, we made use of the equality (7), specialized to each of the phases. Finally, we note that there are n "branches" (one for each phase) to the solution of (30), and that the minimum over all the branches yields the desired lower bound.

Once the minimization problem (30) is solved, an estimate for the associated stress–strain relations may be obtained by simple differentiation with respect to $\bar{\sigma}$. However, by the results of Appendix B, in the computation of the effective stress–strain relations, we may regard the optimization variables $\omega^{(r)}$ and $\eta^{(r)}$ as constants as far as derivatives with respect to $\bar{\sigma}$ are concerned. Thus, the expressions for the effective stress–strain relations may be written in the form:

$$\bar{\varepsilon} = \sum_{\substack{r=1\\ r\neq s}}^{n}\frac{c^{(r)}}{\hat{\tau}_e^{(r)}}\frac{d\psi^{(r)}}{d\tau_e^{(r)}}(\hat{\tau}_e^{(r)})\left[(\hat{\omega}^{(r)})^2\left(\bar{\tau}_p\frac{\partial\bar{\tau}_p}{\partial\bar{\sigma}}+\bar{\tau}_n\frac{\partial\bar{\tau}_n}{\partial\bar{\sigma}}\right)+(\hat{\eta}^{(r)})^2\bar{\tau}_d\frac{\partial\bar{\tau}_d}{\partial\bar{\sigma}}\right]+\cdots$$

$$+\frac{c^{(s)}}{\hat{\tau}_e^{(s)}}\frac{d\psi^{(s)}}{d\tau_e^{(s)}}(\hat{\tau}_e^{(s)})\left[\left((\hat{\omega}^{(s)})^2+\sum_{t=1}^{n}\frac{c^{(t)}}{c^{(s)}}(1-\hat{\omega}^{(t)})^2\right)\left(\bar{\tau}_p\frac{\partial\bar{\tau}_p}{\partial\bar{\sigma}}+\bar{\tau}_n\frac{\partial\bar{\tau}_n}{\partial\bar{\sigma}}\right)+(\hat{\eta}^{(s)})^2\bar{\tau}_d\frac{\partial\bar{\tau}_d}{\partial\bar{\sigma}}\right], \tag{32}$$

where $\hat{\omega}^{(r)}$ and $\hat{\eta}^{(r)}$ are the optimized values of the variables $\omega^{(r)}$ and $\eta^{(r)}$ [from (30)], respectively. The s-phase in the above expression corresponds to the branch attaining the minimum in (30), and the expressions for $\hat{\tau}_e^{(r)} = \tau_e^{(r)}(\hat{\omega}^{(r)},\hat{\eta}^{(r)})$, and $\hat{\tau}_e^{(s)} = \tau_e^{(s)}(\hat{\omega}^{(r)},\hat{\eta}^{(r)})$ are obtained from (31).

The upper estimate for the effective energy function of the nonlinear incompressible fiber composite may be obtained in a similar manner. Thus, the expression for the upper estimate has precisely the same form as the lower bound (30), except that the minimum over all phases is replaced by a maximum. A corresponding estimate for the effective stress–strain relation may also be obtained by means of (32), where, in this case, the s-phase corresponds to the branch attaining the maximum in (30).

The representation (30) for the lower bound (or the upper estimate) involves minimization problems over $2n$ constrained variables. However, the number of optimization variables can be further reduced to $2(n-1)$ unconstrained variables (see Appendix B). For example, in the case of a two-phase, incompressible fiber composite, the optimization constraint may be eliminated by letting $\omega^{(1)} = 1+c^{(2)}\omega$, $\omega^{(2)} = 1-c^{(1)}\omega$, $\eta^{(1)} = 1+c^{(2)}\eta$, and $\eta^{(2)} = 1-c^{(1)}\eta$. In terms of the two unconstrained variables ω and η, the two branches of (30) are

$$\tilde{U}^{(\mathrm{I})}(\bar{\sigma}) = \min_{\omega,\eta}\{c^{(1)}\psi^{(1)}(\sqrt{[(1+c^{(2)}\omega)^2+c^{(2)}\omega^2](\bar{\tau}_p^2+\bar{\tau}_n^2)+(1+c^{(2)}\eta)^2\bar{\tau}_d^2})+\cdots$$

$$+c^{(2)}\psi^{(2)}(\sqrt{(1-c^{(1)}\omega)^2(\bar{\tau}_p^2+\bar{\tau}_n^2)+(1-c^{(1)}\eta)^2\bar{\tau}_d^2})\}, \tag{33}$$

and

$$\tilde{U}^{(\mathrm{II})}(\bar{\sigma}) = \min_{\omega,\eta}\{c^{(1)}\psi^{(1)}(\sqrt{(1+c^{(2)}\omega)^2(\bar{\tau}_p^2+\bar{\tau}_n^2)+(1+c^{(2)}\eta)^2\bar{\tau}_d^2})+\cdots$$

$$+c^{(2)}\psi^{(2)}(\sqrt{[(1-c^{(1)}\omega)^2+c^{(1)}\omega^2](\bar{\tau}_p^2+\bar{\tau}_n^2)+(1-c^{(1)}\eta)^2\bar{\tau}_d^2})\}.$$

Then, the lower bound and the upper estimate are equal to the smallest and the largest of

the two branches, respectively. The corresponding estimates for the effective stress–strain relations are obtained by making appropriate use of (32).

We note that expressions for *lower* bounds on the effective energy functions of *incompressible* nonlinear fiber composites have been obtained previously by Talbot and Willis (1991). These authors made use of the Talbot–Willis variational method, resulting in a different, more complicated, form for the bounds than the form presented here. We also note that expressions (30) for the *lower* bound, and the analogous expression for the *upper* estimate, were first derived by Ponte Castañeda (1992) by application of the variational principle (10). However, the derivation given here, in terms of the identity (C2), is different, and can be generalized to the class of *compressible*, nonlinear fiber composites. This is accomplished in the next section. We also note that expressions (32) for the effective stress–strain relations of the fiber composite are presented here for the first time.

5. COMPRESSIBLE FIBER-REINFORCED COMPOSITES

With the insight gained in the previous section, we attempt in this section to obtain corresponding results for n-phase fiber composites with compressible, nonlinear, isotropic phases. Again, we will make use of the identity (C2) in the expressions for the bounds of the linear comparison composite. Thus, expressions for the lower bound and the upper estimate for the effective energy function of the nonlinear, compressible fiber composite may be obtained by following exactly the same steps that led from (25) to (30).

We begin by making use of the same choice for the optimization variables $\boldsymbol{\Omega}$ as in (27) to rewrite the expression for $\tilde{U}_0^{(\mathrm{HS}-)}$ in terms of the four transversely isotropic invariants of $\bar{\boldsymbol{\sigma}}$: the in-plane hydrostatic stress $\bar{\sigma}_\mathrm{p}$, the normal tensile stress $\bar{\sigma}_\mathrm{n}$, the transverse shear stress $\bar{\tau}_\mathrm{p}$ and the longitudinal shear stress $\bar{\tau}_\mathrm{n}$ (see Appendix A). Next, we observe that the dependence of $\tilde{U}_0^{(HS-)}$ on these four invariants and on the six optimization variables (for each phase) is only through the following $4n$ groups:

$$(\bar{\sigma}_\mathrm{p}\omega_1^{(r)}+\bar{\sigma}_\mathrm{n}\omega_6^{(r)}),\quad (2\bar{\sigma}_\mathrm{p}\omega_5^{(r)}+\bar{\sigma}_\mathrm{n}\omega_2^{(r)}),\quad \bar{\tau}_\mathrm{p}\omega_3^{(r)}\quad\text{and}\quad \bar{\tau}_\mathrm{n}\omega_4^{(r)}. \tag{34}$$

It can be further shown that the $4n$ groups of (34) may be replaced by the $4n$ groups: $\bar{\sigma}_\mathrm{p}\eta^{(r)}$, $\bar{\sigma}_\mathrm{n}\phi^{(r)}$, $\bar{\tau}_\mathrm{p}\omega^{(r)}$ and $\bar{\tau}_\mathrm{n}\theta^{(r)}$, respectively. Consequently, the lower bound for the effective energy function of the linear comparison composite may be rewritten in the form:

$$\begin{aligned}\tilde{U}_0^{(\mathrm{HS}-)}(\bar{\boldsymbol{\sigma}}) = \min_{\Pi}\Bigg\{\sum_{r=1}^{n} c^{(r)}\Bigg[&\frac{1}{2\mu_0^{(r)}}[(\bar{\tau}_\mathrm{p}\omega^{(r)})^2+(\bar{\tau}_\mathrm{n}\theta^{(r)})^2+\tfrac{1}{3}(\bar{\sigma}_\mathrm{p}\eta^{(r)}-\bar{\sigma}_\mathrm{n}\phi^{(r)})^2]+\cdots\\ &+\frac{1}{2\mu_0^{(+)}}[\bar{\sigma}_\mathrm{p}^2(1-\eta^{(r)})^2+\beta_0(\mu_0^{(+)},\kappa_0^{(+)})\bar{\tau}_\mathrm{p}^2(1-\omega^{(r)})^2+\bar{\tau}_\mathrm{n}^2(1-\theta^{(r)})^2]+\cdots\\ &+\frac{1}{2\kappa_0^{(r)}}[\tfrac{2}{3}\bar{\sigma}_\mathrm{p}\eta^{(r)}+\tfrac{1}{3}\bar{\sigma}_\mathrm{n}\phi^{(r)}]^2\Bigg]\Bigg\},\end{aligned} \tag{35}$$

where

$$\beta_0(\mu,\kappa) = 1+\frac{2\mu}{\kappa+\frac{1}{3}\mu}, \tag{36}$$

and where $\Pi = \{\eta^{(r)},\ \phi^{(r)},\ \omega^{(r)},\ \theta^{(r)}\,|\,\bar{\eta}=1,\ \bar{\phi}=1,\ \bar{\omega}=1,\ \bar{\theta}=1\}$ is the reduced set of (constrained) optimization variables. We note that the choice of this set is not unique, and that in some cases, as when $\bar{\sigma}_\mathrm{p}=0$ or $\bar{\sigma}_\mathrm{n}=0$, other choices may be preferred (see Section 6). This is because expression (35) becomes degenerate when $\bar{\sigma}_\mathrm{p}=0$, or $\bar{\sigma}_\mathrm{n}=0$.

With expression (35) for the linear lower bound, relation (21) leads to the following form for the nonlinear lower bound:

$$\tilde{U}^{(\mathrm{HS}-)}(\bar{\boldsymbol{\sigma}}) = \min_{s_1,s_2} \min_{\Pi} \left\{ \sum_{\substack{r=1 \\ r\neq s_1, r\neq s_2}}^{n} c^{(r)} \psi^{(r)}(\tau_{\mathrm{e}}^{(r)}, \sigma_{\mathrm{m}}^{(r)}) + \Delta_0(\bar{\boldsymbol{\sigma}}, \Pi) \right\}, \tag{37}$$

where

$$\tau_{\mathrm{e}}^{(r)} = \sqrt{(\bar{\tau}_{\mathrm{p}}\omega^{(r)})^2 + (\bar{\tau}_{\mathrm{n}}\theta^{(r)})^2 + \tfrac{1}{3}(\bar{\sigma}_{\mathrm{p}}\eta^{(r)} - \bar{\sigma}_{\mathrm{n}}\phi^{(r)})^2}, \tag{38}$$

$$\sigma_{\mathrm{m}}^{(r)} = \tfrac{2}{3}\bar{\sigma}_{\mathrm{p}}\eta^{(r)} + \tfrac{1}{3}\bar{\sigma}_{\mathrm{n}}\phi^{(r)},$$

and where

$$\begin{aligned}\Delta_0 = \max_{\mu_0^{(s_1)}, \kappa_0^{(s_2)} \geqslant 0} \Bigg\{ & \sum_{I=1}^{n} \frac{c^{(I)}}{2\mu_0^{(s_1)}} [\bar{\sigma}_{\mathrm{p}}^2(1-\eta^{(I)})^2 + \beta_0(\mu_0^{(s_1)}, \kappa_0^{(s_2)})\bar{\tau}_{\mathrm{p}}^2(1-\omega^{(I)})^2 + \bar{\tau}_{\mathrm{n}}^2(1-\theta^{(I)})^2] + \cdots \\ & + c^{(s_1)} \left[\frac{1}{2\mu_0^{(s_1)}} (\tau_{\mathrm{e}}^{(s_1)})^2 + \max_{\tau_{\mathrm{e}}} \left\{ \frac{1}{2\mu_0^{(s_1)}} \tau_{\mathrm{e}}^2 - \psi^{(s_1)}(\tau_{\mathrm{e}}, \sigma_{\mathrm{m}}^{(s_1)}) \right\} \right] + \cdots \\ & + c^{(s_2)} \left[\frac{1}{2\kappa_0^{(s_2)}} (\sigma_{\mathrm{m}}^{(s_2)})^2 + \max_{\sigma_{\mathrm{m}}} \left\{ \frac{1}{2\kappa_0^{(s_2)}} \sigma_{\mathrm{m}}^2 - \psi^{(s_2)}(\tau_{\mathrm{e}}^{(s_2)}, \sigma_{\mathrm{m}}) \right\} \right] \Bigg\}. \end{aligned} \tag{39}$$

Here, we have made use of the Saddle Point Theorem to interchange the order of the minimum over the set Π with the maximum over the comparison moduli $\mu_0^{(r)}$ and $\kappa_0^{(r)}$. We have also made use of relation (7) specialized to each of the phases to simplify the above expression. However, it should be noted that relation (7) cannot be used in (39) due to the coupling between the two optimization variables $\mu_0^{(s_1)}$ and $\kappa_0^{(s_2)}$. The representation (37) involves a minimization problem over $4n$ constrained variables, along with the intermediate four-dimensional optimization problem (39). However, the constraint can be easily embedded in (37) to reduce the dimension of the optimization problem to $4(n-1)$ (see Appendix B). Finally, we note that the problem (37) has n^2 branches (one for each possible combination of $\mu_0^{(s_1)}$ and $\kappa_0^{(s_2)}$, $s_1, s_2 = 1, \ldots, n$), and that the lower bound is then obtained by taking the minimum over all these branches.

The upper estimate for the effective energy function of the compressible, nonlinear fiber composite may be obtained in a similar manner. Thus, the expression for the upper estimate has precisely the same form as that for the lower bound (37), except that the minimum over all possible combinations of $\mu_0^{(s_1)}$ and $\kappa_0^{(s_2)}$ is replaced by a maximum.

On the face of it, the representation (37) for the lower bound (or the upper estimate) for the effective energy function of the nonlinear fiber composite does not appear to offer much of an advantage over the previous representation (21). However, in many practical applications, associated with special classes of fiber-reinforced composites, further simplification of the above representation is possible. For example, if a particular phase, say phase s, is stiffer (weaker) than the others, only one branch of the solution needs to be evaluated since, in this case, the choice $s_1 = s_2 = s$ leads to the lower bound (upper estimate). Further, we note that whenever the intermediate optimization problem (39) can be solved analytically, the representation (37) is preferable because it involves a simple minimization problem, in contrast with expression (21) which requires the solution of a minimax problem. From a computational point of view, this eliminates the need for the iterative procedure associated with the evaluation of the functions $V^{(r)}$ in (21). To illustrate this point, let us examine the class of compressible fiber composites with one or more incompressible phases.

Thus, we consider a compressible, n-phase fiber composite, with at least one incompressible phase. Then, the trivial choice $\kappa_0^{(s_2)} = \infty$ attains the minimum in (37). This further allows the evaluation of the optimization problem (39). The lower bound reduces to the $3n$-dimensional constrained minimization problem:

$$\tilde{U}^{(HS-)}(\bar{\boldsymbol{\sigma}}) = \min_{s} \min_{\substack{\omega^{(r)},\bar{\omega}=1 \\ \phi^{(r)},\bar{\phi}=1 \\ \eta^{(r)},\bar{\eta}=1}} \left\{ \sum_{\substack{r=1 \\ r\neq s}}^{n} c^{(r)}\psi^{(r)}(\tau_e^{(r)}, \sigma_m^{(r)}) + c^{(s)}\psi^{(s)}(\tau_e^{(s)}, \sigma_m^{(s)}) \right\}, \tag{40}$$

where

$$\tau_e^{(r)} = \sqrt{(\bar{\tau}_p^2+\bar{\tau}_n^2)(\omega^{(r)})^2 + \tfrac{1}{3}(\bar{\sigma}_p\eta^{(r)} - \bar{\sigma}_n\phi^{(r)})^2}, \quad (r = 1,\ldots,n;\ r\neq s), \tag{41}$$

$$\tau_e^{(s)} = \sqrt{(\bar{\tau}_p^2+\bar{\tau}_n^2)(\omega^{(s)})^2 + \tfrac{1}{3}(\bar{\sigma}_p\eta^{(s)} - \bar{\sigma}_n\phi^{(s)})^2 + \sum_{t=1}^{n} \frac{c^{(t)}}{c^{(s)}}[\bar{\sigma}_p^2(1-\eta^{(t)})^2 + (\bar{\tau}_p^2+\bar{\tau}_n^2)(1-\omega^{(t)})^2]},$$

and

$$\sigma_m^{(r)} = \tfrac{2}{3}\bar{\sigma}_p\eta^{(r)} + \tfrac{1}{3}\bar{\sigma}_n\phi^{(r)}, \ (r = 1,\ldots,n).$$

Within this class of composites, the sub-class of hollow-fiber composites (for which the above expression for the lower bound reduces to a simple, explicit result) is of particular interest. Thus, we take the complementary energy-density function of the matrix (phase 1) to be of the form $U^{(1)}(\boldsymbol{\sigma}) = \psi(\tau_e)$. Correspondingly, the complementary energy-density function of the cylindrical voids (phase 2) is given by $U^{(2)}(\boldsymbol{\sigma}) = \infty$ if $\boldsymbol{\sigma} \neq \mathbf{0}$, and 0 otherwise. The minimum in (40) is trivially attained by the choice $s = 1$ and $\omega^{(2)} = \phi^{(2)} = \eta^{(2)} = 0$. The values of the variables $\omega^{(1)}$, $\phi^{(1)}$ and $\eta^{(1)}$ then follow from the optimization constraint. Substitution of these values into (40), leads to the following expression for the lower bound for the hollow-fiber composites

$$\tilde{U}^{(HS-)}(\bar{\boldsymbol{\sigma}}) = (1-c)\psi\left(\frac{1}{(1-c)}\sqrt{(1+c)(\bar{\tau}_p^2+\bar{\tau}_n^2) + \tfrac{1}{3}(\bar{\sigma}_p-\bar{\sigma}_n)^2 + c\bar{\sigma}_p^2}\right), \tag{42}$$

where $c = c^{(2)}$ is the volume fraction of the voids. The corresponding estimate for the stress–strain relation may be derived with the help of (A12). We note that when $\psi(\tau_e) = a(\tau_e)^{n+1}$, where a is a non-negative constant and $n > 1$, the above result reduces to the lower bound derived independently by Suquet (1992) for power-law materials containing cylindrical voids. [The more general result (42) is also given by Suquet (1992).]

Another class of composites, of great practical significance, for which the representation of the lower bound may be simplified, by explicit evaluation of (39), is the class of n-phase fiber composites for which the stiffest phase is linear. In the following section, we deal with the special case of two-phase, fiber-reinforced composites of this type.

6. APPLICATION TO METAL-MATRIX COMPOSITES

Among the various classes of fiber-reinforced composites, the class of metal-matrix composites is one of the most common. In this section, we restrict our attention to this important class of composites, which are made up of ductile matrices reinforced by stiffer, linear-elastic fibers. Since the plastic strains in the metal phase are independent of the hydrostatic stresses, we assume that the behavior of the matrix (phase 1) is governed by a complementary energy-density function of the form:

$$\psi^{(1)}(\tau_e, \sigma_m) = \varphi(\tau_e) + \frac{1}{2\kappa^{(1)}}\sigma_m^2, \tag{43}$$

where the function φ is non-negative and satisfies the strong convexity assumption described in Section 2, and where $\kappa^{(1)}$ is the usual bulk modulus. Further, to account for the initial linear-elastic behavior in shear of the metal phase, we assume that $\varphi(\tau_e) = \dfrac{1}{2\mu^{(1)}}\tau_e^2 + f(\tau_e)$,

where $\mu^{(1)}$ is the elastic shear modulus. On the other hand, the behavior of the fiber material (phase 2) is governed by the quadratic complementary energy-density function

$$\psi^{(2)}(\tau_e, \sigma_m) = \frac{1}{2\mu^{(2)}}\tau_e^2 + \frac{1}{2\kappa^{(2)}}\sigma_m^2, \tag{44}$$

where $\mu^{(2)}$ and $\kappa^{(2)}$ are the corresponding shear and bulk moduli, respectively. Finally, to enforce the assumption that phase 2 is stiffer than phase 1, we let $\mu^{(2)} > \mu^{(1)}$ and $\kappa^{(2)} > \kappa^{(1)}$.

We begin by considering the lower bound $\tilde{U}^{(HS-)}$. As mentioned in the previous section, since phase 2 is linear and stiffer than phase 1, the intermediate optimization (39) may be evaluated explicitly. Further, because of the particular choice for the energy-density functions $\psi^{(1)}$ and $\psi^{(2)}$, a different choice for the reduced set of optimization variables in (34) leads to additional simplification of the problem. Thus, with the new choice for the optimization variables, the lower bound for the effective energy function of the composite may be given in terms of the following 3-dimensional minimization problem

$$\tilde{U}^{(HS-)}(\bar{\sigma}) = \min_{\eta,\omega,\theta}\left\{c^{(1)}\left[\varphi(\tau_e^{(1)}) + \frac{1}{2\kappa^{(1)}}(\sigma_m^{(1)})^2\right] + c^{(2)}\left[\frac{1}{2\mu^{(2)}}(\tau_e^{(2)})^2 + \frac{1}{2\kappa^{(2)}}(\sigma_m^{(2)})^2\right]\right\}, \tag{45}$$

where

$$\begin{aligned}
(\tau_e^{(1)})^2 &= \bar{\tau}_p^2(1+c^{(2)}\omega)^2 + \bar{\tau}_n^2(1+c^{(2)}\theta)^2 + \tfrac{1}{3}(\bar{\sigma}_p - \bar{\sigma}_n)^2(1+c^{(2)}\eta)^2,\\
(\tau_e^{(2)})^2 &= \bar{\tau}_p^2[(1-c^{(1)}\omega)^2 + c^{(1)}\beta_0(\mu_0^{(2)}, \kappa_0^{(2)})\omega^2] + \bar{\tau}_n^2[(1-c^{(1)}\theta)^2 + c^{(1)}\theta^2] + \cdots\\
&\quad + \tfrac{1}{3}(\bar{\sigma}_p - \bar{\sigma}_n)^2(1-c^{(1)}\eta)^2 + c^{(1)}[\tfrac{1}{3}\bar{\sigma}_p(2\phi+\eta) + \tfrac{1}{3}\bar{\sigma}_n(\phi-\eta)]^2,\\
\sigma_m^{(1)} &= (\tfrac{2}{3}\bar{\sigma}_p + \tfrac{1}{3}\bar{\sigma}_n)(1+c^{(2)}\phi),\\
\sigma_m^{(2)} &= (\tfrac{2}{3}\bar{\sigma}_p + \tfrac{1}{3}\bar{\sigma}_n)(1-c^{(1)}\phi).
\end{aligned} \tag{46}$$

In the above expression, β_0 is given by relation (36) and

$$\phi = \frac{\bar{\sigma}_p\left(\dfrac{2}{\kappa^{(2)}} - \dfrac{2}{\kappa^{(1)}} - \dfrac{\eta}{\mu^{(2)}}\right) + \bar{\sigma}_n\left(\dfrac{1}{\kappa^{(1)}} - \dfrac{1}{\kappa^{(2)}} + \dfrac{\eta}{\mu^{(2)}}\right)}{(2\bar{\sigma}_p + \bar{\sigma}_n)\left(\dfrac{c^{(2)}}{\kappa^{(1)}} + \dfrac{c^{(1)}}{\kappa^{(2)}} + \dfrac{1}{\mu^{(2)}}\right)}. \tag{47}$$

Once the minimization problem (45) is solved, the corresponding estimate for the effective stress–strain relation may be obtained by following the same procedure followed for the incompressible fiber composite. Thus, the estimate for the stress–strain relation may be written in the form

$$\bar{\varepsilon} = \frac{\partial}{\partial\bar{\sigma}}\left\{c^{(1)}\left[\varphi(\hat{\tau}_e^{(1)}) + \frac{1}{2\kappa^{(1)}}(\hat{\sigma}_m^{(1)})^2\right] + c^{(2)}\left[\frac{1}{2\mu^{(2)}}(\hat{\tau}_e^{(2)})^2 + \frac{1}{2\kappa^{(2)}}(\hat{\sigma}_m^{(2)})^2\right]\right\}, \tag{48}$$

where $\hat{\tau}_e^{(1)}, \hat{\tau}_e^{(2)}, \hat{\sigma}_m^{(1)}$ and $\hat{\sigma}_m^{(2)}$ are evaluated from (46) at the optimal values of η, ω and θ. Further, in (48), the derivatives with respect to $\bar{\sigma}$ are evaluated with η, ω and θ fixed. We emphasize that due to the different choice of the optimization variables, the above representation for the lower bound is subject to the restrictions $(2\bar{\sigma}_p + \bar{\sigma}_n) \neq 0$ and $(\bar{\sigma}_p - \bar{\sigma}_n) \neq 0$ [instead of the restrictions $\bar{\sigma}_p \neq 0$ and $\bar{\sigma}_n \neq 0$, for the representation (37)]. For consistency, we will make use of the same set of optimization variables in the following representation for the upper estimate, although, in this case, the number of the optimization variables cannot be reduced (from 4 to 3).

The evaluation of the upper estimate is more complicated since in this case the inter-

mediate optimization problem (39) cannot be solved explicitly. However, if the ratio of the initial shear modulus to the bulk modulus of the weaker, matrix phase is small (i.e. $\mu^{(1)}/\kappa^{(1)} \ll 1$), significant simplification may be achieved by means of the following approximation for β_0, namely,

$$\beta_0(\mu_0^{(1)}, \kappa_0^{(1)}) = 1 + 2\frac{\mu_0^{(1)}}{\kappa_0^{(1)}} + o\left[\left(\frac{\mu_0^{(1)}}{\kappa_0^{(1)}}\right)^2\right]. \tag{49}$$

Then, the estimate for the upper bound for the effective energy function reduces to

$$\tilde{U}^{(\mathrm{HS}+)}(\bar{\boldsymbol{\sigma}}) \cong \min_{\eta,\phi,\omega,\theta} \left\{ c^{(1)}\left[\varphi(\tau_e^{(1)}) + \frac{1}{2\kappa^{(1)}}(\sigma_m^{(1)})^2\right] + c^{(2)}\left[\frac{1}{2\mu^{(2)}}(\tau_e^{(2)})^2 + \frac{1}{2\kappa^{(2)}}(\sigma_m^{(2)})^2\right]\right\}, \tag{50}$$

where

$$\begin{aligned}
(\tau_e^{(1)})^2 &= \bar{\tau}_p^2[(1+c^{(2)}\omega)^2 + c^{(2)}\omega^2] + \bar{\tau}_n^2[(1+c^{(2)}\theta)^2 + c^{(2)}\theta^2] + \cdots \\
&\quad + \tfrac{1}{3}(\bar{\sigma}_p - \bar{\sigma}_n)^2(1+c^{(2)}\eta)^2 + c^{(2)}[\tfrac{1}{3}\bar{\sigma}_p(2\phi+\eta) + \tfrac{1}{3}\bar{\sigma}_n(\phi-\eta)]^2, \\
(\tau_e^{(2)})^2 &= \bar{\tau}_p^2(1-c^{(1)}\omega)^2 + \bar{\tau}^2(1-c^{(1)}\theta)^2 + \tfrac{1}{3}(\bar{\sigma}_p - \bar{\sigma}_n)^2(1-c^{(1)}\eta)^2, \\
(\sigma_m^{(1)})^2 &= (\tfrac{2}{3}\bar{\sigma}_p + \tfrac{1}{3}\bar{\sigma}_n)^2(1+c^{(2)}\phi)^2 + 2c^{(1)}\bar{\tau}_p^2\omega^2, \\
\sigma_m^{(2)} &= (\tfrac{2}{3}\bar{\sigma}_p + \tfrac{1}{3}\bar{\sigma}_n)(1-c^{(1)}\phi).
\end{aligned} \tag{51}$$

We recall that (50) is subject to the restrictions $(2\bar{\sigma}_p + \bar{\sigma}_n) \neq 0$ and $(\bar{\sigma}_p - \bar{\sigma}_n) \neq 0$. Also, we remark that, fortunately, the approximation (49) holds for most metal matrix composites. For example, when $\mu^{(1)}/\kappa^{(1)} < 0.45$ (or in terms of the associated Poisson's ratio, $\nu^{(1)} > 0.3$), the maximum difference between (50) and the exact solution of the expression for $\tilde{U}^{(\mathrm{HS}+)}$ is only about 2% (see Fig. 3). Finally, we note that when $\bar{\tau}_p = 0$ the two forms are equal.

The associated expressions for the stress–strain relations may be evaluated from the upper estimate for the effective energy function in the usual way. Thus, the expressions for the effective stress–strain relations have the same form as (48), but with $\hat{\tau}_e^{(1)}$, $\hat{\tau}_e^{(2)}$, $\hat{\sigma}_m^{(1)}$ and $\hat{\sigma}_m^{(2)}$ evaluated from (51) at the optimal values of the variables η, ϕ, ω and θ [from (50)].

We conclude this section by noting that the lower bound (45) is actually an optimal bound (i.e. no bound that is better can be given for this class of composites). This can be shown by following arguments analogous to those given by Ponte Castañeda (1991b) in the context of statistically isotropic, two-phase, nonlinear composites with one linear phase. From a more practical point of view, however, the above results for the lower bound may be used as estimates for the effective energy functions of two-phase composites with ductile, nonlinear fibers embedded in a linear-elastic matrix (see Section 3). Alternatively, the upper estimate (50), together with the corresponding estimate for the stress–strain relations, serve as estimates for the behavior of composites with a ductile matrix reinforced by stiffer, linear-elastic fibers.

We note that the class of microstructures associated with the upper estimates (for the effective energy functions) correspond to those typical of metal-matrix composites. This suggests that the predictions for the effective stress–strain relation obtained from the upper estimate $\tilde{U}^{(\mathrm{HS}+)}$ could be used as estimates for the effective behavior of metal-matrix composites. Indeed, the study of the effective behavior of an aluminum-matrix composite, that is carried out in the next section, confirms this expectation.

7. APPLICATION TO AN ALUMINUM-MATRIX COMPOSITE REINFORCED WITH BORON FIBERS

In this section, we specialize the results of the previous section to the case of a nonlinear, compressible, fiber composite made up of an aluminum-matrix reinforced with boron fibers. The effective behavior of the composite is presented in terms of relations between the four

transversely isotropic stress modes and the corresponding four strain modes (see Appendix A). These relations show the overall response of the anisotropic composite to different loading modes and reveal the coupling among the different modes.

Aluminum (phase 1) is a ductile material with a uniaxial stress–strain curve that can be approximated by a "linear-plus-power" law [see Fig. 2 in Adams (1970)]. Accordingly, we assume the following form for the energy-density function of the aluminum matrix:

$$\psi^{(1)}(\tau_e, \sigma_m) = \varepsilon_0 \int_0^{\sqrt{3}\tau_e} \left[\frac{s}{\sigma_0} + \left(\frac{s}{\sigma_0} - \frac{\sigma_y}{\sigma_0} \right)^n H(s-\sigma_y) \right] ds + \frac{1}{2\kappa^{(1)}} \sigma_m^2. \tag{52}$$

Here, H is the unit step function (equal to 0 when $s \leqslant \sigma_y$, or to 1 otherwise) and ε_0 and σ_0 are the strain and stress normalization factors, respectively, such that $\sigma_0/\varepsilon_0 = 3\mu^{(1)}$, with $\mu^{(1)}$ denoting the elastic shear modulus. Also, $\kappa^{(1)}$ is the bulk modulus and σ_y is the yield stress in tension. Boron (phase 2) is a brittle material that behaves linearly up to failure. Its energy-density function is given by (44), with $\mu^{(2)}$ and $\kappa^{(2)}$ denoting the shear and bulk modulus of boron, respectively.

The lower bound and the upper estimate for the effective energy function of the composite may then be represented in dimensionless form via the relation:

$$\frac{\tilde{U}^{(HS\mp)}}{\sigma_0 \varepsilon_0}(\bar{\sigma}) = G^{(\mp)} \left\{ \frac{\bar{\sigma}_p}{\sigma_0}, \frac{\bar{\sigma}_n}{\sigma_0}, \frac{\bar{\tau}_p}{\sigma_0}, \frac{\bar{\tau}_n}{\sigma_0}; \frac{\sigma_y}{\sigma_0}, \frac{\mu^{(2)}}{\mu^{(1)}}, \nu^{(1)}, \nu^{(2)}, n, c^{(2)} \right\}, \tag{53}$$

where $G^{(-)}$ and $G^{(+)}$ are obtained from (45) and (50), respectively. The Poisson's ratios of the two phases $\nu^{(1)}$ and $\nu^{(2)}$ are defined by

$$\nu^{(r)} = \frac{3\kappa^{(r)} - 2\mu^{(r)}}{6\kappa^{(r)} + 2\mu^{(r)}} \quad (r = 1, 2). \tag{54}$$

The corresponding estimates for the four transversely isotropic strain modes are then determined by making use of (48) along with (A5).

The numerical values for the six parameters in (54) are chosen so that a comparison with the corresponding experimental results of Adams (1970) may be carried out. Thus, the properties of the aluminum matrix are taken from Fig. 2 in Adams (1970), which presents the uniaxial stress–strain curve for the aluminum. Similarly, the numerical values for the elastic constants of the boron fibers, as well as their volume fraction, were also taken from the same reference. These parameters are

$$\frac{\sigma_y}{\sigma_0} = 14.9, \quad \frac{\mu^{(2)}}{\mu^{(1)}} = 7.47, \quad \nu^{(1)} = 0.32, \quad \nu^{(2)} = 0.20, \quad n = 1.82 \quad \text{and} \quad c^{(2)} = 0.34,$$

where $\sigma_0 = 5.89$ MPa and $\varepsilon_0 = 9.29 \times 10^{-5}$ are the appropriate normalization factors.

Results for the different loading modes of the nonlinear fiber composites, under several loading combinations, are given in Figs 2, 4, 5 and 6. To highlight the effect of nonlinearlity, results are also given in the form of short-dash curves for linear fiber composites with the same elastic properties as the nonlinear fiber composite. Thus, the phases of these linear *reference* composites are identical to those of the nonlinear composite with the only difference being that σ_y is taken to be unbounded for phase 1.

Figure 2 shows a plot of the normalized transverse shear stress $\bar{\tau}_p/\tau_y$ versus the normalized transverse shear strain $\bar{\gamma}_p/\gamma_y$ for three different loading combinations. Here, $\tau_y = \sigma_y/\sqrt{3}$ and $\gamma_y = \tau_y/2\mu^{(1)}$ denote the yield stress and strain in shear of the aluminum matrix, respectively. The continuous curves correspond to estimates derived from the lower bound for the effective energy function, while the long-dash curves correspond to estimates derived from the upper estimate for the effective energy function. For all three loading combinations, $\bar{\sigma}_p = 0$. The curves denoted by $\bar{\sigma}_n/\bar{\tau}_p = \bar{\tau}_n/\bar{\tau}_p = 0$ correspond to a pure transverse shear load. Initially, the behaviors of these two stress–strain curves for the nonlinear composites are

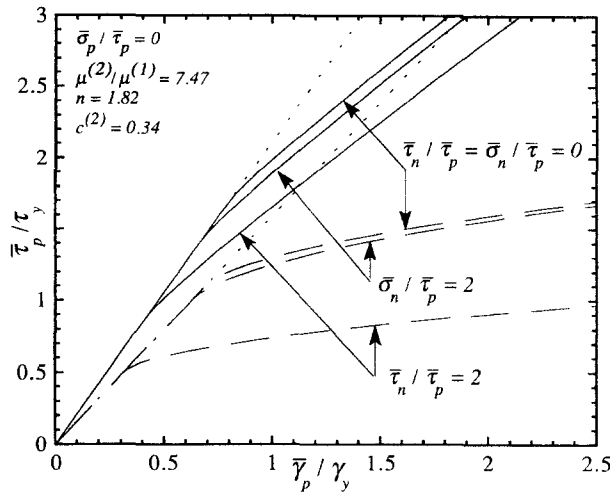

Fig. 2. Lower estimates (continuous curves) and upper estimates (long-dash curves) for the relations between the transverse shear stress $\bar{\tau}_p$ and the corresponding shear strain $\bar{\gamma}_p$ of the nonlinear fiber composites, as well as for the reference linear fiber composites (short-dash lines), for three different loading combinations: $\bar{\sigma}_n/\bar{\tau}_p = \bar{\tau}_n/\bar{\tau}_p = 0$, $\bar{\tau}_n/\bar{\tau}_p = 2$ and $\bar{\sigma}_n/\bar{\tau}_p = 2$. Here, $\bar{\sigma}_p = 0$ in all cases.

the same as those of the corresponding curves for the reference linear composites (short-dash lines). However, the predictions for the effective yield points of the two types of estimates are different, with both the yield stresses and the yield strains being larger for the estimate associated with the lower bound on the energy.

The effective stress–strain relations associated with the lower energy bound show post-yield behavior with almost linear hardening with a slope approaching the value

$$\frac{2c^{(2)}\mu^{(2)}(\kappa^{(2)}+\frac{1}{3}\mu^{(2)})}{(2-c^{(2)})\kappa^2+\frac{1}{3}(8-7c^{(2)})\mu^{(2)}}. \tag{55}$$

The corresponding stress–strain relation for the upper energy estimate shows post-yield behavior with power hardening, where the growth of the strain is proportional to $(\bar{\tau}_n/\tau_y)^n$ for large $\bar{\tau}_n$.

As discussed in the previous section, the stress–strain relations derived from the upper estimate for the effective energy function may be used as estimates for the behavior of composites with a ductile matrix phase and linear-elastic fibers. In this context, it is interesting to compare our results with the corresponding predictions of Hashin (1980) [see also Dvorak and Bahei-El-Din (1987)], who argues, on physical grounds, the existence of two distinct failure modes for fiber-reinforced composites with a weaker matrix phase : a *fiber*-dominated mode in which the composite fails due to fiber failure in tension or compression along the fibers, and a *matrix*-dominated mode in which the matrix fails in shear transverse to, or along, the fibers. According to this model, when the composite is subjected to transverse shear loads, its yield stress and post-yield behavior are dominated by the behavior of the ductile matrix. We note that our predictions for the behavior of the composite, from the stress–strain curve associated with the upper energy estimate, are consistent with Hashin's model. Thus, our results indicate that the effective yield stress is only slightly higher than the yield stress of the matrix, and that the post-yield behavior is dominated by the behavior of the ductile matrix as well.

The coupling between the shear modes $\bar{\tau}_n$ and $\bar{\tau}_p$ is illustrated by the two curves for the proportional loading path $\bar{\tau}_n/\bar{\tau}_p = 2$, and the coupling between $\bar{\sigma}_n$ and $\bar{\tau}_p$ by the two curves for the proportional loading path $\bar{\sigma}_n/\bar{\tau}_p = 2$. We note that the effect of a combination of transverse shear loads with any of the other modes is to saturate the linear range of phase 1, accelerating the onset of yield in the composite. Thus, the resistance of the composite to transverse shear loads is reduced by application of any of the other loading modes. We note that this softening effect is more marked for the stress–strain curves obtained from the

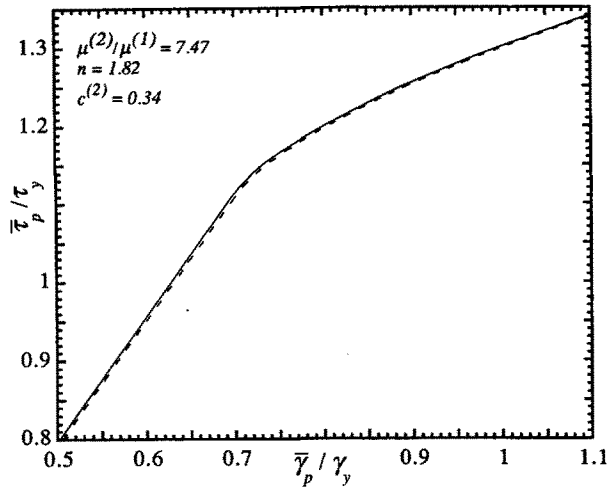

Fig. 3. Comparison of the upper estimate for the relations between the transverse shear stress $\bar{\tau}_p$ and the corresponding shear strain $\bar{\gamma}_p$ (continuous curve), with the corresponding approximation (50), based on neglecting terms of order $(\mu_0^{(1)}/\kappa_0^{(1)})^2$ (short-dash curve).

upper energy estimate. Also, the coupling effect of the superimposed longitudinal shear $\bar{\tau}_n$ on the transverse shear mode $\bar{\tau}_p$ is more pronounced than that of the superimposed uniaxial tensile stress $\bar{\sigma}_n$.

To illustrate the consequences of this softening phenomenon, let us consider a cylindrical fiber composite bar, subjected to a uniaxial tension load in the fiber direction combined with a torque aligned with the symmetry axis. At the local level, the stress field that develops within this bar may be represented by a combination of a uniaxial tensile stress $\bar{\sigma}_n$ and the transverse shear stress $\bar{\tau}_p$. Thus, our results predict that any increment in the uniaxial tensile stress (with fixed transverse shear stress) will cause additional growth of the resultant transverse shear strain. The overall contributions of the shear strain increments (within the composite) is to increase the twist angle of the bar. Thus, at the global level, our results would predict an increase of the twist angle in response to an increment in the tensile load (with a fixed applied torque).

Figure 3 shows a plot of the normalized shear stress $\bar{\tau}_p/\tau_y$ versus the normalized shear strain $\bar{\gamma}_p/\gamma_y$, in the vicinity of the predicted yield point, when all other stress modes vanish. Here, we compare the predictions for $\bar{\gamma}_p$ obtained from the exact solution for the minimax problem [see (37)–(39)] for $\tilde{U}^{(HS+)}$ (continuous curves) with the corresponding approximation (50) (short-dash curve), based on neglecting terms of order $(\mu_0^{(1)}/\kappa_0^{(1)})^2$. As we can see, the two curves are very close, with a maximum error of about 0.5%. We note that the maximum error between the two curves always occurs near the predicted yield points.

Figure 4 shows a plot of the normalized longitudinal shear stress $\bar{\tau}_n/\tau_y$ versus the normalized longitudinal shear strain $\bar{\gamma}_n/\gamma_y$ for three different loading combinations. The continuous curves correspond to the estimates derived from the lower bound for the effective energy function, while the long-dash curves correspond to the estimates derived from the upper estimate for the effective energy function. For all three loading combinations, $\bar{\sigma}_p = 0$.

The curves denoted by $\bar{\tau}_p/\bar{\tau}_n = \bar{\sigma}_n/\bar{\tau}_n = 0$ correspond to a pure longitudinal shear load along the fibers. We observe that the predictions for the yield stresses, the yield strains and the post-yield behaviors obtained from the upper energy estimates are very similar to the predictions of the corresponding curve in Fig. 2 (denoted by $\bar{\sigma}_n/\bar{\tau}_p = \bar{\tau}_n/\bar{\tau}_p = 0$). This similarity is anticipated on grounds of our previous observation concerning the interpretation of the upper energy estimates as estimates for ductile-matrix composites. Thus, when the ductile-matrix composite is subjected to shear loads along the fibers, it is expected that its yield and post-yield behaviors will be dominated by the corresponding behaviors of the ductile matrix, and hence the similarity between the upperbound energy curves in the Figs 2 and 4.

On the other hand, the curves associated with the lower bounds, in Figs 2 and 4, are

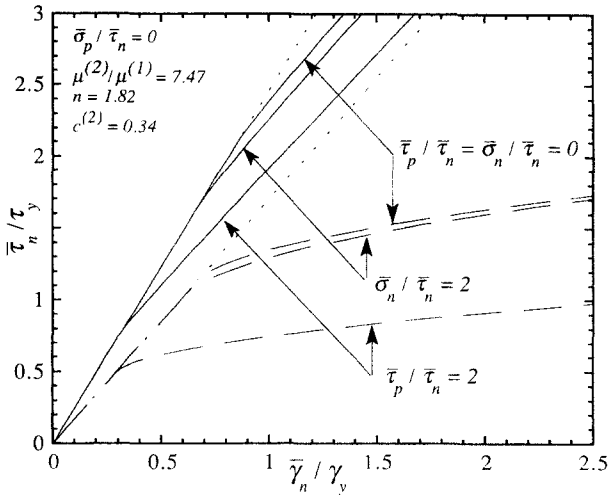

Fig. 4. Lower estimates (continuous curves) and upper estimates (long-dash curves) for the relations between the longitudinal shear stress $\bar{\tau}_n$ and the corresponding shear strain $\bar{\gamma}_n$ of the nonlinear fiber composites, as well as for the reference linear fiber composites (short-dash lines), for three different loading combinations: $\bar{\sigma}_n/\bar{\tau}_n = \bar{\tau}_p/\bar{\tau}_n = 0$, $\bar{\tau}_p/\bar{\tau}_n = 2$ and $\bar{\sigma}_n/\bar{\tau}_n = 2$. Here, $\bar{\sigma}_p = 0$ in all cases.

not as close. Although the post-yielding behavior is nearly linear for both cases, there is a significant difference between the asymptotic slopes of the curves as the stress increases. In Fig. 4, the slope of the longitudinal shear stress–strain curve approaches the value $2c^{(2)}\mu^{(2)}/(2-c^{(2)})$, whereas the corresponding slope for the transverse shear stress curve, in Fig. 2, approaches a lower value, given by relation (55).

The coupling between the shear modes $\bar{\tau}_n$ and $\bar{\tau}_p$ is illustrated by two curves for the proportional loading path $\bar{\tau}_p/\bar{\tau}_n = 2$, whereas the coupling between $\bar{\sigma}_n$ and $\bar{\tau}_p$ is illustrated by the two curves for the proportional loading path $\bar{\sigma}_n/\bar{\tau}_n = 2$. We observe that the superposition of any of the other modes on the longitudinal shear mode has the effect of saturating earlier the linear range of phase 1, thus increasing the apparent ductility of the composite. Therefore, analogously to the previous case (Fig. 2), the resistance of the composite to longitudinal shear loads is reduced with the addition of any of the other loading modes.

Figure 5 shows plots of the normalized tensile stress $\bar{\sigma}_n/\sigma_y$ versus the normalized tensile strain $\bar{\varepsilon}_n/\varepsilon_y$ for three different loading combinations. Here, $\varepsilon_y = \sigma_y/2\mu^{(1)}(1+\nu^{(1)})$ denotes

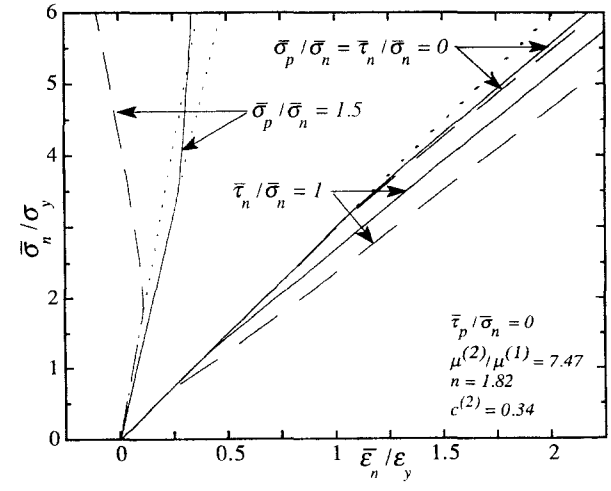

Fig. 5. Lower estimates (continuous curves) and upper estimates (long-dash curves) for the relations between the normal tensile stress $\bar{\sigma}_n$ and the corresponding strain $\bar{\varepsilon}_n$ of the nonlinear fiber composites, as well as for the reference linear fiber composites (short-dash lines), for three different loading combinations: $\bar{\sigma}_p/\bar{\sigma}_n = \bar{\tau}_n/\bar{\sigma}_n = 0$, $\bar{\sigma}_p/\bar{\sigma}_n = 1.5$ and $\bar{\tau}_n/\bar{\sigma}_n = 1$. Here, $\bar{\tau}_p = 0$ in all cases.

the yield strain of the aluminum matrix under uniaxial tensile load. The continuous curves correspond to the estimates derived from the lower bound for the effective energy function, while the long-dash curves correspond to the estimates derived from the upper estimate for the effective energy function. For all three loading combinations, $\bar{\tau}_p = 0$.

The curves denoted by $\bar{\sigma}_p/\bar{\sigma}_n = \bar{\tau}_n/\bar{\sigma}_n = 0$ correspond to a uniaxial tensile load in the fiber direction. Initially, the behaviors of the two curves are the same as those of the reference linear composite (short-dash lines), until phase 1 yields. The predictions for the effective yield stress and strain are almost the same, and after yielding, the plastic hardening of both estimates for the composite is nearly linear. As discussed by Hashin (1980), this post-yield behavior is expected on physical grounds since the stiff phase dominates the behavior of the composite in tension (or compression) along the fibers.

The coupling between the two dilatational modes is illustrated by the two curves for the proportional loading path $\bar{\sigma}_p/\bar{\sigma}_n = 1.5$. Thus, we see that the superimposed $\bar{\sigma}_p$ leads to significant stiffening of the composite. We observe that the two curves (for $\bar{\sigma}_p/\bar{\sigma}_n = 1.5$) are initially fairly close to each other (and behave the same way as the corresponding curves of the reference linear composites). However, after yielding of phase 1, the predictions based on the upper energy estimate are markedly different from the corresponding predictions from the lower energy bound. Thus, the lower energy bound predicts only little growth of the tensile strain; while the corresponding upper energy estimate actually predicts a *decrease* of the normal tensile strain. This interesting behavior is due to the plastic incompressibility of the aluminum phase. Because the plastic strains in phase 1 are proportional to the stress deviators, and under the above combination of loads, the normal component of the stress deviator (in the fiber direction) is negative, the plastic part of the normal tensile strain decreases. According to the lower bound, the magnitudes of the elastic and the plastic parts of the tensile strain are almost the same, and hence $\bar{\varepsilon}_n$ (the sum of the two parts) is almost fixed. However, according to the upper estimate, under these loading conditions, the magnitude of the plastic part of the tensile strain is larger than that of the elastic part, and hence $\bar{\varepsilon}_n$ decreases.

The coupling between the normal tensile stress and the longitudinal shear stress $\bar{\tau}_n$ is illustrated by the two curves corresponding to the proportional loading path $\bar{\tau}_n/\bar{\sigma}_n = 1$. The effect of increasing the shear load $\bar{\tau}_n$ is to saturate earlier the linear range of phase 1, hence increasing the apparent ductility of the composite. We note that the difference between the curves for the lower bound and the upper estimate is relatively small in this case.

Figure 6 shows plots of the normalized in-plane hydrostatic stress $\bar{\sigma}_p/\sigma_y$ versus the normalized in-plane hydrostatic strain $\bar{\varepsilon}_p/\varepsilon_y$ for three different loading combinations. The

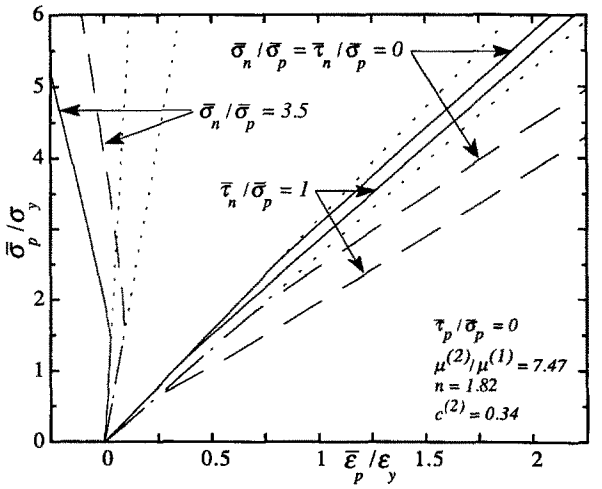

Fig. 6. Lower estimates (continuous curves) and upper estimates (long-dash curves) for the relations between the in-plane hydrostatic stress $\bar{\sigma}_p$ and the corresponding strain $\bar{\varepsilon}_p$ of the nonlinear fiber composites, as well as for the reference linear fiber composites (short-dash lines), for three different loading combinations: $\bar{\sigma}_n/\bar{\sigma}_p = \bar{\tau}_n/\bar{\sigma}_p = 0$, $\bar{\sigma}_n/\bar{\sigma}_p = 3.5$ and $\bar{\tau}_n/\bar{\sigma}_p = 1$. Here, $\bar{\tau}_p = 0$ in all cases.

continuous curves correspond to the estimates derived from the lower bound for the effective energy function, while the long-dash curves to the estimates derived from the upper estimate for the effective energy function. For all three loading combinations, $\bar{\tau}_p = 0$.

The curves denoted by $\bar{\sigma}_n/\bar{\sigma}_p = \bar{\tau}_n/\bar{\sigma}_p = 0$ correspond to a pure, plane hydrostatic load in the transverse direction. Initially, the behaviors of the two curves are the same as those of the reference linear composite (short-dash lines), until the yielding of phase 1. After yielding, both types of estimates predict linear hardening for the composites. This suggests that the in-plane hydrostatic strains are governed by the stiff linear phase. In the case of normal tensile loads (Fig. 5), it is easy to visualize that the tensile mode (along the fibers) should be controlled by the stiffer phase; however, that the same behavior should also be observed for the in-plane hydrostatic strains is perhaps less intuitive. The reasoning lies in the Poisson effect: when the fiber composite is subjected to in-plane hydrostatic loads, tensile strains are set up in the fiber direction (due to the Poisson effect), which must be continuous across the phases, thus providing the required stiffening effect in the transverse direction (because the linear phase controls the strains along the fibers).

The coupling between the two dilatational modes is illustrated by the two curves for the proportional loading path $\bar{\sigma}_n/\bar{\sigma}_p = 3.5$. We observe that the two curves have the same behaviors as the corresponding curves for the reference linear composite (short-dash lines), until phase 1 yields. After yielding, however, the in-plane hydrostatic strain decreases for both types of estimates. The reasons for this have already been discussed in the context of Fig. 5. The curves for the proportional loading path $\bar{\tau}_n/\bar{\sigma}_n = 1$ show relatively weak coupling between the in-plane hydrostatic stress and the longitudinal shear stress $\bar{\tau}_n$. These curves resemble the corresponding curves for $\bar{\tau}_n/\bar{\sigma}_n = 1$ in Fig. 5.

Finally, we make a comparison between our theoretical results and the experimental data of Adams (1970). For definiteness, we consider a Cartesian coordinate frame, where the x_3 axis is aligned with the fiber direction **n**, and the other two axes lie in the transverse plane (see Fig. 1). We make use of the results of Appendix A to determine the values of the four transversely isotropic stress (strain) invariants in terms of the Cartesian components for a given stress (strain) tensor. In this case, the applied load $\bar{\sigma}_{22}$ is a tensile stress in the transverse direction, and we have $\bar{\sigma}_p = \frac{1}{2}\bar{\sigma}_{22}$, $\bar{\tau}_p = \frac{1}{2}\bar{\sigma}_{22}$. Therefore, by means of the chain rule, the corresponding tensile strain component is

$$\bar{\varepsilon}_{22} = \frac{\partial \tilde{U}}{\partial \bar{\sigma}_{22}} = \bar{\varepsilon}_p + \bar{\gamma}_p.$$

Figure 7 shows plots of the transverse tensile stress $\bar{\sigma}_{22}$ versus the plastic part of the

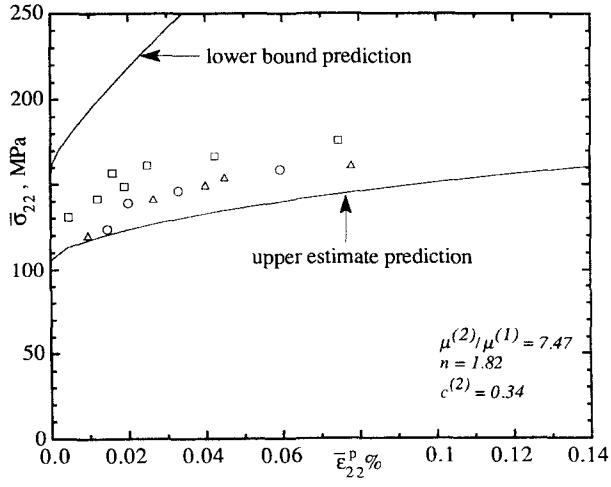

Fig. 7. Lower and upper estimates (continuous curves) for the relations between the uniaxial tensile stress $\bar{\sigma}_{22}$ and the uniaxial plastic tensile strain $\bar{\varepsilon}^p_{22}$ for the nonlinear fiber composite, and results for three sets of experimental data points (squares, triangles and circles), corresponding to three tests carried out on an aluminum-matrix composite reinforced with boron fibers (Adams, 1970).

corresponding tensile strain $\bar{\varepsilon}^{\mathrm{p}}_{22}$. Three sets of experimental data points are shown (squares, triangles and circles), representing the three different tests carried out on the aluminum-matrix composite (Adams, 1970). Two curves representing the corresponding two estimates obtained from the lower bound and the upper estimate for the effective energy function are also shown. We observe that the two curves bound the experimental data points from above and below. However, the curve obtained from the upper energy estimate is much closer to the experimental data points. This is in agreement with our prior discussions suggesting that the stress–strain relations derived from the upper energy estimate can be used as estimates for the behavior of two-phase fiber composites with the ductile phase playing the role of the matrix and the brittle phase that of the fibers.

8. CONCLUDING REMARKS

In this work, we have obtained bounds and estimates for the effective behavior of nonlinear fiber-reinforced composites by means of a variational procedure introduced by Ponte Castañeda (1991a, 1992). This procedure enabled the extension of lower and upper bounds of the Hashin–Shtrikman (1962) type for the effective energy functions of n-phase *linear* fiber-reinforced composites to corresponding lower bounds and upper estimates (estimates for the upper bound) for the effective energy functions of n-phase *nonlinear* fiber composites. Simple representations for these bounds and estimates, generalizing earlier results by Ponte Castañeda (1992) for the class of *incompressible* fiber composites, were obtained for the class of *compressible* fiber composites. We note that different, but equivalent, expressions for the *lower* bound for the effective energy functions of *incompressible* fiber composites have also been obtained previously by Talbot and Willis (1991), using a different procedure. However, the form of the lower bounds obtained in this work is simpler. Additionally, the more practically useful *upper* estimates of the Hashin–Shtrikman type are also new. In particular, these upper estimates have not been available by the Talbot-Willis method.

The important case of compressible, two-phase fiber composites made up of a ductile and a brittle phase was studied in detail. The general expression for the lower bound was specialized for this class of composites, and a similar expression, based on neglecting terms of order $(\mu_0^{(1)}/\kappa_0^{(1)})^2$, was obtained for the upper estimate. Corresponding estimates for the effective stress–strain relations were obtained by straightforward differentiation of these expressions. Explicit calculations were carried out for an aluminum-boron system, highlighting the significant couplings that may arise between the different loading modes.

Finally, we proposed alternative (approximate) interpretations for the constitutive relations derived from the lower bounds and upper estimates for the effective energy functions of two-phase, nonlinear fiber composites. Thus, the results based on the lower bounds were given the interpretation of estimates for the effective behavior of fiber composites made up of stiffer linear-elastic matrices weakened by ductile fibers. Correspondingly, the results based on the upper estimates for the effective energy functions were given the interpretation of estimates for the effective behavior of fiber composites made up of ductile matrices reinforced by stiffer linear-elastic fibers. This latter interpretation was confirmed through comparison with available experimental results for a metal-matrix, fiber-reinforced composite.

Acknowledgements—This work was supported by the Air Force Office of Scientific Research (Grant No. 91-0161). The authors wish to thank Mr Kingshuk Bose for his valuable comments on an earlier version of the paper.

REFERENCES

Adams, D. F. (1970). Inelastic analysis of a unidirectional composite subjected to transverse normal loading. *J. Compos. Mater.* **4**, 310–328.

Budiansky, B. (1959). A reassessment of deformation theories of plasticity. *J. Appl. Mech., Trans. ASME* **81**, 259–264.

de Buhan, P., Salencon, J. and Taliercio, A. (1990). Lower and upper bound estimates for the macroscopic strength criterion of fiber composite material. In *Inelastic Deformation of Composite Materials* (Edited by G. J. Dvorak), pp. 563–580. Springer, New York.

deBotton, G. and Ponte Castañeda, P. (1992). On the ductility of laminated materials. *Int. J. Solids Structures* **29**, 2329–2353.
Drucker, D. C. (1959). On minimum weight design and strength of non-homogeneous plastic bodies. In *Non-homogeneity in Elasticity and Plasticity* (Edited by W. Olszak), pp. 139–146. Pergamon Press, New York.
Dvorak, G. J. and Bahei-El-Din, Y. A. (1987). A bimodal plasticity theory of fibrous composite material. *Acta Mech.* **69**, 219–241.
Dvorak, G. J., Bahei-El-Din, Y. A., Macheret, Y. and Liu, C. H. (1988). An experimental study of elastic–plastic behavior of a fibrous Boron–Aluminum composite. *J. Mech. Phys. Solids* **36**, 655–687.
Hashin, Z. (1965). On the elastic behavior of fiber reinforced materials of arbitrary transverse phase geometry. *J. Mech. Phys. Solids* **13**, 119–134.
Hashin, Z. (1972). Theory of fiber reinforced materials. NASA CR-1974.
Hashin, Z. (1980). Failure criteria for unidirectional fiber composites. *J. Appl. Mech.* **47**, 329–334.
Hashin, Z. (1983). Analysis of composite materials—a survey. *J. Appl. Mech.* **50**, 481–505.
Hashin, Z., Bagchi, D. and Rosen, B. W. (1974). Non-linear behavior of fiber composite laminates. NASA CR-2313.
Hashin, Z. and Shtrikman, S. (1962). On some variational principles in anisotropic and nonhomogeneous elasticity. *J. Mech. Phys. Solids* **10**, 335–342.
Hill, R. (1963). Elastic properties of reinforced solids: some theoretical principles. *J. Mech. Phys. Solids* **11**, 357–372.
Hill, R. (1964a). Theory of mechanical properties of fiber-strengthened materials: I. Elastic behavior. *J. Mech. Phys. Solids* **12**, 199–213.
Hill, R. (1964b). Theory of mechanical properties of fiber-strengthened materials: II. Inelastic behavior. *J. Mech. Phys. Solids* **12**, 214–218.
Hill, R. (1965). A self consistent mechanics of composite materials. *J. Mech. Phys. Solids* **13**, 213–222.
Hill, R. (1967). The essential structure of constitutive laws for metal composites and polycrystals. *J. Mech. Phys. Solids* **15**, 79–95.
Leblond, J. B., Perrin, G. and Suquet, P. (1993). Exact results and approximate models for porous viscoplastic solids. *Int. J. Plasticity* (to appear).
Lipton, R. (1991). On the behavior of elastic composites with transverse isotropic symmetry. *J. Mech. Phys. Solids* **39**, 663–681.
Lipton, R. (1992). Bounds and perturbation series for incompressible elastic composites with transverse isotropic symmetry. *J. Elasticity* **27**, 193–225.
Majumdar, S. and McLaughlin, P. V. (1975). Effects of phase geometry and volume fraction on the plane stress limit analysis of a unidirectional fiber-reinforced composite. *Int. J. Solids Structures* **11**, 771–791.
Mehrabadi, M. M. and Cowin, S. T. (1990). Eigentensors of linear anisotropic elastic materials. *Q. J. Mech. Appl. Math.* **43**, 15–41.
Mori, T. and Tanaka, K. (1973). Average stress in the matrix and average elastic energy of materials with misfitting inclusions. *Acta Metall.* **21**, 571–574.
Ponte Castañeda, P. (1991a). The effective mechanical properties of nonlinear isotropic composites. *J. Mech. Phys. Solids* **39**, 45–71.
Ponte Castañeda, P. (1991b). The effective properties of brittle/ductile incompressible composites. In *Inelastic Deformation of Composite Materials* (Edited by G. J. Dvorak), pp. 215–231. Springer, New York.
Ponte Castañeda, P. (1992). New variational principles in plasticity and their application to composites materials. *J. Mech. Phys. Solids* **40**, 1757–1788.
Ponte Castañeda, P. and deBotton, G. (1992). On the homogenized yield strength of two-phase composites. *Proc. R. Soc. Lond. A* **438**, 419–431.
Rockafellar, R. T. (1970). *Convex Analysis*. Princeton University Press, Princeton, NJ.
Shu, L. S., and Rosen, B. W. (1967). Strength of fiber-reinforced composites by limit analysis methods. *J. Compos Mater.* **1**, 366–381.
Spencer, A. J. M. (1971). Theory of invariants. In *Continuum Physics, Vol. 1* (Edited by A. C. Eringen), pp. 239–353. Academic Press, New York.
Sun, C. T. and Chen, J. L. (1991). A micromechanical model for plastic behavior of fibrous composites. *Compos. Sci. Tech.* **40**, 115–129.
Suquet, P. (1987). Elements of homogenization for inelastic solid mechanics. In *Homogenization Techniques for Composite Media, Lecture Notes in Physics 272* (Edited by E. Sanchez-Palencia and A. Zaoui), pp. 193–278. Springer, New York.
Suquet, P. (1992). On bounds for the overall potential of power law materials containing voids with an arbitrary shape. *Mech. Res. Comm.* **19**, 51–58.
Talbot, D. R. S. and Willis, J. R. (1985). Variational principles for inhomogeneous nonlinear media. *IMA. J. Appl. Math.* **35**, 39–54.
Talbot, D. R. S. and Willis, J. R. (1991). The overall behavior of a nonlinear fiber reinforced composite. In *Inelastic Deformation of Composite Materials* (Edited by G. J. Dvorak), pp. 527–545. Springer, New York.
Talbot, D. R. S. and Willis, J. R. (1992). Some explicit bounds for the overall behavior of nonlinear composites. *Int. J. Solids Structures* **29**, 1981–1987.
Walpole, L. J. (1969). On the overall elastic moduli of composite materials. *J. Mech. Phys. Solids* **17**, 235–251.
Walpole, L. J. (1981). Elastic behavior of composite materials: Theoretical foundations. In *Advances in Applied Mechanics* (Edited by C. S. Yih), pp. 169–242. Academic Press, New York.
Willis, J. R. (1981). Variational and related methods for the overall properties of composites. In *Advances in Applied Mechanics* (Edited by C. S. Yih), pp. 1–78. Academic Press, New York.
Willis, J. R. (1982). Elasticity theory of composites. In *Mechanics of Solids, the Rodney Hill 60th Anniversary Volume* (Edited by H. G. Hopkins and M. J. Sewell), pp. 653–686. Pergamon Press, New York.
Willis, J. R. (1983). The overall response of composite materials. *ASME J. Appl. Mech.* **50**, 1202–1209.
Zhao, Y. H. and Weng, G. J. (1990). Theory of plasticity for a class of inclusion and fiber-reinforced composites. In *Micromechanics and Inhomogeneity, The Toshio Mura Anniversary Volume* (Edited by G. J. Weng, M. Taya and H. Abé), pp. 599–622. Springer, New York.

APPENDIX A: ON THE CHARACTERIZATION OF TRANSVERSELY ISOTROPIC MATERIALS

The purpose of this appendix is to gather some results relevant to the analysis of materials with transversely isotropic symmetry. These results are used extensively throughout the body of the paper in the development of estimates for the effective behavior of nonlinear fiber composites, which constitute a special class of transversely isotropic materials. The emphasis of this section is on representations for the transversely isotropic invariants of the stress and strain tensors. The reason is that *nonlinear* transversely isotropic materials are most efficiently characterized in terms of energy-density functions depending on these invariants.

A.1. *Isotropic invariants*

As is well-known, there are three isotropic invariants for a symmetric, second-order tensor. However, only two of these, which are of quadratic order or less, are relevant to linear-elastic behavior. These invariants may be expressed [see, for example, Walpole (1981)] in terms of two fourth-order *projection* tensors $\mathbf{J}$ and $\mathbf{K}$, such that $\mathbf{I}=\mathbf{J}+\mathbf{K}$, $\mathbf{J}=\mathbf{JJ}$, $\mathbf{K}=\mathbf{KK}$ and $\mathbf{JK}=\mathbf{0}$. Their Cartesian components are given by

$$J_{ijkl}=\tfrac{1}{3}\delta_{ij}\delta_{kl},\quad K_{ijkl}=\tfrac{1}{2}(\delta_{ik}\delta_{jl}+\delta_{il}\delta_{jk}-\tfrac{2}{3}\delta_{ij}\delta_{kl}), \tag{A1}$$

where δ_{ij} is the Kronecker delta symbol. Then, in terms of these projection tensors, we define two isotropic invariants of the stress tensor via

$$\sigma_{\mathrm{m}}=\tfrac{1}{3}J_{kkij}\sigma_{ij}\quad\text{and}\quad\tau_{\mathrm{e}}^2=\tfrac{1}{2}K_{ijkl}\sigma_{ij}\sigma_{kl}, \tag{A2}$$

called the hydrostatic (mean) stress, and the effective shear stress, respectively. We also define the hydrostatic strain ε_{m}, and the effective shear strain γ_{e} by relations analogous to (A2).

It is important to note that the elasticity tensor $\mathbf{L}$ of an isotropic, linear-elastic material admits a spectral decomposition

$$\mathbf{L}=3\kappa\mathbf{J}+2\mu\mathbf{K}, \tag{A3}$$

where $\mathbf{J}$ and $\mathbf{K}$ play the role of the eigenprojections, and the bulk and shear moduli of the material, κ and μ, are the corresponding eigenvalues.

A.2. *Transversely isotropic invariants*

There are in general five transversely isotropic invariants of a symmetric, second-order tensor (Spencer, 1971). However, only four of these invariants are linear, or quadratic, in order. They may be represented in terms of the four projection tensors (Walpole, 1981) $\mathbf{E}^{[1]}$, $\mathbf{E}^{[2]}$, $\mathbf{E}^{[3]}$ and $\mathbf{E}^{[4]}$, satisfying the relations $\mathbf{E}^{[p]}\mathbf{E}^{[p]}=\mathbf{E}^{[p]}$; $\mathbf{E}^{[p]}\mathbf{E}^{[q]}=\mathbf{0}$, $p\neq q$; and $\mathbf{E}^{[1]}+\mathbf{E}^{[2]}+\mathbf{E}^{[3]}+\mathbf{E}^{[4]}=\mathbf{I}$. The Cartesian components of these four projection tensors are given by:

$$\begin{aligned}
E^{[1]}_{ijkl}&=\tfrac{1}{2}\beta_{ij}\beta_{kl},\\
E^{[2]}_{ijkl}&=\alpha_{ij}\alpha_{kl},\\
E^{[3]}_{ijkl}&=\tfrac{1}{2}(\beta_{ik}\beta_{jl}+\beta_{jk}\beta_{il}-\beta_{ij}\beta_{kl}),\\
E^{[4]}_{ijkl}&=\tfrac{1}{2}(\beta_{ik}\alpha_{jl}+\beta_{il}\alpha_{jk}+\beta_{jl}\alpha_{ik}+\beta_{jk}\alpha_{il}),
\end{aligned} \tag{A4}$$

where $\alpha_{ij}=n_in_j$ and $\beta_{ij}=\delta_{ij}-n_in_j$, with $\mathbf{n}$ denoting the axis of transverse isotropy. Then, the four transversely isotropic invariants of the stress tensor $\boldsymbol{\sigma}$ may be expressed in the forms:

$$\begin{aligned}
\sigma_{\mathrm{p}}&=\tfrac{1}{2}E^{[1]}_{iikl}\sigma_{kl}=\tfrac{1}{2}\sigma_{ij}\beta_{ij}, && \{\tfrac{1}{2}(\sigma_{11}+\sigma_{22})\},\\
\sigma_{\mathrm{n}}&=E^{[2]}_{iikl}\sigma_{kl}=\sigma_{ij}\alpha_{ij}, && \{\sigma_{33}\},\\
\tau_{\mathrm{p}}^2&=\tfrac{1}{2}\sigma_{ij}E^{[3]}_{ijkl}\sigma_{kl}=\tfrac{1}{2}[\sigma_{ij}\sigma_{kl}\beta_{ik}\beta_{lj}-\tfrac{1}{2}(\sigma_{ij}\beta_{ij})^2], && \{\sigma_{12}^2+\tfrac{1}{4}(\sigma_{11}-\sigma_{22})^2\},\\
\tau_{\mathrm{n}}^2&=\tfrac{1}{2}\sigma_{ij}E^{[4]}_{ijkl}\sigma_{kl}=[\sigma_{ij}\sigma_{ki}\alpha_{jk}-(\sigma_{ij}\alpha_{ij})^2], && \{(\sigma_{13}^2+\sigma_{23}^2)\}.
\end{aligned} \tag{A5}$$

Physically, these invariants correspond to the in-plane hydrostatic stress, the normal tensile stress, the (in-plane) transverse shear stress, and the (anti-plane) longitudinal shear stress (given in parentheses are the corresponding representations for a choice of $\mathbf{n}$ aligned with the 3-direction). Analogous relations apply for the transversely isotropic invariants of the strain tensor $\boldsymbol{\varepsilon}$, denoted respectively by ε_{p}, ε_{n}, γ_{p} and γ_{n}. We also note for latter reference that the following relations hold between the transversely isotropic invariants of (A5) and the isotropic invariants of (A2),

$$\sigma_{\mathrm{m}}=\tfrac{1}{3}(2\sigma_{\mathrm{p}}+\sigma_{\mathrm{n}}),\quad\tau_{\mathrm{e}}^2=\tau_{\mathrm{p}}^2+\tau_{\mathrm{n}}^2+\tfrac{1}{3}(\sigma_{\mathrm{p}}-\sigma_{\mathrm{n}})^2. \tag{A6}$$

Contrary to the situation for isotropic materials, the above four projection tensors are not the eigentensors of the spectral decomposition of an arbitrary transversely isotropic elasticity tensor (Mehrabadi and Cowin, 1990). Such eigentensors would involve the material moduli. Therefore, it is necessary to introduce (Walpole, 1981) two other tensors, that are *not* projections, $\mathbf{E}^{[5]}$ and $\mathbf{E}^{[6]}$, with components

$$E^{[5]}_{ijkl}=\alpha_{ij}\beta_{kl}\quad\text{and}\quad E^{[6]}_{ijkl}=\beta_{ij}\alpha_{kl}. \tag{A7}$$

The elasticity tensor $\mathbf{L}$ of an arbitrary transversely isotropic material may be expressed in terms of these six tensors, via

$$\mathbf{L} = a_1\mathbf{E}^{[1]} + a_2\mathbf{E}^{[2]} + a_3\mathbf{E}^{[3]} + a_4\mathbf{E}^{[4]} + a_5(\mathbf{E}^{[5]} + \mathbf{E}^{[6]}), \tag{A8}$$

where a_q ($q = 1, \ldots, 5$) are the five moduli that suffice to characterize the behavior of the material. The compliance tensor $\mathbf{M}$, of an arbitrary transversely isotropic material may be expressed in a similar form. It is worth mentioning that the isotropic projection $\mathbf{J}$, can be represented in the form

$$\mathbf{J} = \tfrac{2}{3}\mathbf{E}^{[1]} + \tfrac{1}{3}\mathbf{E}^{[2]} + \tfrac{1}{3}(\mathbf{E}^{[5]} + \mathbf{E}^{[6]}), \tag{A9}$$

and that we can additionally define, for later reference, the tensor $\mathbf{E}'$ such that

$$\mathbf{E}' = \mathbf{E}^{[3]} + \mathbf{E}^{[4]} - \mathbf{K}. \tag{A10}$$

The tensor $\mathbf{E}'$ is a projection tensor, orthogonal to $\mathbf{E}^{[3]}$ and $\mathbf{E}^{[4]}$.

Finally, we remark that the energy density function of a transversely isotropic, linear-elastic material may be represented in the form

$$U(\boldsymbol{\sigma}) = \psi(\sigma_{\mathrm{p}}, \sigma_{\mathrm{n}}, \tau_{\mathrm{p}}, \tau_{\mathrm{n}}). \tag{A11}$$

Then, the relations between the transversely isotropic stress and strain invariants are given by

$$\varepsilon_{\mathrm{p}} = \frac{1}{2}\frac{\partial\psi}{\partial\sigma_{\mathrm{p}}}, \quad \varepsilon_{\mathrm{n}} = \frac{\partial\psi}{\partial\sigma_{\mathrm{n}}}, \quad \gamma_{\mathrm{p}} = \frac{1}{2}\frac{\partial\psi}{\partial\tau_{\mathrm{p}}} \quad \text{and} \quad \gamma_{\mathrm{n}} = \frac{1}{2}\frac{\partial\psi}{\partial\tau_{\mathrm{n}}}. \tag{A12}$$

A.3. *Incompressible, transversely isotropic invariants*

For incompressible, transversely isotropic materials, it suffices to consider the three invariants of quadratic order or less, on the space of traceless, symmetric, second-order tensors. These may be obtained in terms of the three orthogonal projection tensors $\mathbf{E}^{[3]}$, $\mathbf{E}^{[4]}$ and $\mathbf{E}'$, defined in the previous subsection. Thus, the incompressible, transversely isotropic invariants of the stress tensor $\boldsymbol{\sigma}$ are τ_{p}, τ_{n}, and the deviatoric (axisymmetric) shear stress

$$\tau_{\mathrm{d}} = \frac{1}{\sqrt{3}}(\sigma_{\mathrm{p}} - \sigma_{\mathrm{n}}), \tag{A13}$$

corresponding to the three above projections, respectively. We note that from $(A6)_2$ we have the following identity relating the effective shear stress and the incompressible, transversely isotropic invariants, $\tau_{\mathrm{e}}^2 = \tau_{\mathrm{p}}^2 + \tau_{\mathrm{n}}^2 + \tau_{\mathrm{d}}^2$. The corresponding strain invariants are denoted γ_{p}, γ_{n} and γ_{d}.

Finally, we note that the elasticity tensor $\mathbf{L}$ of an incompressible, transversely isotropic, linear-elastic material admits a spectral decomposition of the form

$$\mathbf{L} = 2\mu_{\mathrm{p}}\mathbf{E}^{[3]} + 2\mu_{\mathrm{n}}\mathbf{E}^{[4]} + 2\mu_{\mathrm{d}}\mathbf{E}', \tag{A14}$$

where μ_{p}, μ_{n}, μ_{d} are the three shear moduli characterizing the behavior of such a material (Lipton, 1992).

APPENDIX B: ESTIMATES FOR THE EFFECTIVE STRESS–STRAIN RELATIONS

In this appendix, we demonstrate the process of obtaining estimates for the effective stress–strain relations of nonlinear fiber composites from corresponding expressions for bounds and estimates for the effective energy functions, which are given in the body of the paper. We begin by considering expression (21) for the lower bound for the effective energy function. Since all the phases in the composite are assumed to be isotropic, the functions $V^{(r)}$ in expression (21) may be written in the form

$$V^{(r)}(\mu_0^{(r)}, \kappa_0^{(r)}) = \max_{\tau_{\mathrm{e}}^{(r)},\, \sigma_{\mathrm{m}}^{(r)}} \left\{ \frac{1}{2\mu_0^{(r)}}(\tau_{\mathrm{e}}^{(r)})^2 + \frac{1}{2\kappa_0^{(r)}}(\sigma_{\mathrm{m}}^{(r)})^2 - \psi^{(r)}(\tau_{\mathrm{e}}^{(r)}, \sigma_{\mathrm{m}}^{(r)}) \right\}. \tag{B1}$$

Assuming sufficient smoothness for the functions $\psi^{(r)}$, the corresponding optimization conditions can be expressed in terms of the following $2n$ implicit equations for the variables $\tau_{\mathrm{e}}^{(r)}$ and $\sigma_{\mathrm{m}}^{(r)}$,

$$\frac{1}{\mu_0^{(r)}}\tau_{\mathrm{e}}^{(r)} - \frac{\partial\psi^{(r)}}{\partial\tau_{\mathrm{e}}^{(r)}}(\tau_{\mathrm{e}}^{(r)}, \sigma_{\mathrm{m}}^{(r)}) = 0 \quad \text{and} \quad \frac{1}{\kappa_0^{(r)}}\sigma_{\mathrm{m}}^{(r)} - \frac{\partial\psi^{(r)}}{\partial\sigma_{\mathrm{m}}^{(r)}}(\tau_{\mathrm{e}}^{(r)}, \sigma_{\mathrm{m}}^{(r)}) = 0, \tag{B2}$$

and we denote by $\hat{\tau}_{\mathrm{e}}^{(r)}(\mu_0^{(r)}, \kappa_0^{(r)})$ and $\hat{\sigma}_{\mathrm{m}}^{(r)}(\mu_0^{(r)}, \kappa_0^{(r)})$ the solutions for these equations. Then, substitution of the solutions for $V^{(r)}$ into (21), leads to

$$\tilde{U}^{(\mathrm{HS}-)}(\bar{\boldsymbol{\sigma}}) = \max_{\mu_0^{(r)},\, \kappa_0^{(r)} \geqslant 0} \{F(\bar{\boldsymbol{\sigma}}; \mu_0^{(r)}, \kappa_0^{(r)})\}, \tag{B3}$$

where

$$F = \left[\frac{1}{2}\bar{\sigma}_{ij}(\tilde{M}_0^{(\mathrm{HS}-)})_{ijkl}\bar{\sigma}_{kl} - \sum_{r=1}^{n} c^{(r)} \left[\frac{1}{2\mu_0^{(r)}}(\hat{\tau}_{\mathrm{e}}^{(r)})^2 + \frac{1}{2\kappa_0^{(r)}}(\hat{\sigma}_{\mathrm{m}}^{(r)})^2 - \psi^{(r)}(\hat{\tau}_{\mathrm{e}}^{(r)}, \hat{\sigma}_{\mathrm{m}}^{(r)}) \right] \right]. \tag{B4}$$

Once again, the optimization conditions for the above problem can be stated in terms of $2n$ equations for the variables $\mu_0^{(r)}$ and $\kappa_0^{(r)}$, namely,

$$\frac{\partial F(\bar{\boldsymbol{\sigma}};\mu_0^{(r)},\kappa_0^{(r)})}{\partial \mu_0^{(r)}}=0 \quad \text{and} \quad \frac{\partial F(\bar{\boldsymbol{\sigma}};\mu_0^{(r)},\kappa_0^{(r)})}{\partial \kappa_0^{(r)}}=0. \tag{B5}$$

We denote the optimal values of the variables $\mu_0^{(r)}$ and $\kappa_0^{(r)}$, satisfying (B5), by $\hat{\mu}_0^{(r)}(\bar{\boldsymbol{\sigma}})$ and $\hat{\kappa}_0^{(r)}(\bar{\boldsymbol{\sigma}})$, respectively. In terms of these optimal values, the lower bound for the effective energy function may be expressed in the form

$$\tilde{U}^{(\mathrm{HS}-)}(\bar{\boldsymbol{\sigma}})=F(\bar{\boldsymbol{\sigma}};\hat{\mu}_0^{(r)},\hat{\kappa}_0^{(r)}), \tag{B6}$$

and the corresponding estimate for the stress–strain relations is given by

$$\begin{aligned}\bar{\varepsilon}_{ij}&=\frac{\partial \tilde{U}^{(\mathrm{HS}-)}(\bar{\boldsymbol{\sigma}})}{\partial \sigma_{ij}}\\&=[\tilde{M}_0^{(\mathrm{HS}-)}(\hat{\mu}_0^{(r)},\hat{\kappa}_0^{(r)})]_{ijkl}\bar{\sigma}_{kl}+\sum_{r=1}^{n}\frac{\partial F(\bar{\boldsymbol{\sigma}};\hat{\mu}_0^{(r)},\hat{\kappa}_0^{(r)})}{\partial \mu_0^{(r)}}\frac{\partial \hat{\mu}_0^{(r)}(\bar{\boldsymbol{\sigma}})}{\partial \sigma_{ij}}+\sum_{r=1}^{n}\frac{\partial F(\bar{\boldsymbol{\sigma}};\hat{\mu}_0^{(r)},\hat{\kappa}_0^{(r)})}{\partial \kappa_0^{(r)}}\frac{\partial \hat{\kappa}_0^{(r)}(\bar{\boldsymbol{\sigma}})}{\partial \sigma_{ij}}.\end{aligned} \tag{B7}$$

However, due to the optimization conditions (B5), the last two sums in (B7) vanish, and the estimate (22) for the effective stress–strain relations is obtained. Analogous expressions for the upper estimate, effective stress–strain relations may be obtained similarly.

Next, we consider the estimate for effective stress–strain relations (32), obtained from the lower bound for the effective energy function of the incompressible fiber composite (30). For simplicity, we assume that the nth branch attains the minimum in (30) (e.g. $s=n$), and additionally we define $\bar{\tau}^2=\bar{\tau}_{\mathrm{p}}^2+\bar{\tau}_{\mathrm{n}}^2$. Then, the optimization constraints $\bar{\omega}=1$ and $\bar{\eta}=1$ may be eliminated by letting

$$\omega^{(n)}=\frac{1}{c^{(n)}}\left[1-\sum_{r=1}^{n-1}c^{(r)}\omega^{(r)}\right] \quad \text{and} \quad \eta^{(n)}=\frac{1}{c^{(n)}}\left[1-\sum_{r=1}^{n-1}c^{(r)}\eta^{(r)}\right]. \tag{B8}$$

In terms of the $2(n-1)$ optimization variables $\omega^{(r)}$, $\eta^{(r)}$ $(r=1,\ldots,n-1)$, expression (30) may be rewritten in the form

$$\tilde{U}^{(\mathrm{HS}-)}(\bar{\boldsymbol{\sigma}})=\min_{\substack{\omega^{(r)},\eta^{(r)}\\ r=1,\ldots,n-1}}\left\{\sum_{t=1}^{n-1}c^{(t)}\psi^{(t)}(\tau_{\mathrm{e}}^{(t)})+c^{(n)}\psi^{(n)}(\tau_{\mathrm{e}}^{(n)})\right\}, \tag{B9}$$

where the variables $\tau_{\mathrm{e}}^{(r)}$ $(r=1,\ldots,n-1)$ are given by relation $(31)_1$, and

$$\tau_{\mathrm{e}}^{(n)}=\sqrt{\bar{\tau}^2\left[1+2\left(\frac{1}{c^{(n)}}-\sum_{t=1}^{n-1}\frac{c^{(t)}}{c^{(n)}}\omega^{(t)}\right)^2-\sum_{t=1}^{n}\frac{c^{(t)}}{c^{(n)}}(1-(\omega^{(t)})^2)\right]+\bar{\tau}_{\mathrm{d}}^2\left(\frac{1}{c^{(n)}}-\sum_{t=1}^{n-1}\frac{c^{(t)}}{c^{(n)}}\eta^{(t)}\right)^2}. \tag{B10}$$

It follows that the $2(n-1)$ optimization conditions in (B9) are given by the relations

$$\frac{1}{\tau_{\mathrm{e}}^{(r)}}(\psi^{(r)})'(\tau_{\mathrm{e}}^{(r)})\omega^{(r)}+\frac{1}{\tau_{\mathrm{e}}^{(n)}}(\psi^{(n)})'(\tau_{\mathrm{e}}^{(n)})\left[\omega^{(n)}-\frac{2}{c^{(n)}}\left(1-\sum_{t=1}^{n-1}c^{(t)}\omega^{(t)}\right)\right]=0, \tag{B11}$$

and

$$\frac{1}{\tau_{\mathrm{e}}^{(r)}}(\psi^{(r)})'(\tau_{\mathrm{e}}^{(r)})\eta^{(r)}+\frac{1}{c^{(n)}\tau_{\mathrm{e}}^{(n)}}(\psi^{(n)})'(\tau_{\mathrm{e}}^{(n)})\left(1-\sum_{t=1}^{n-1}c^{(t)}\eta^{(t)}\right)=0.$$

If we now denote the optimal values of $\omega^{(r)}$ and $\eta^{(r)}$, satisfying (B11), by $\hat{\omega}^{(r)}$ and $\hat{\eta}^{(r)}$, respectively, the lower bound for the effective energy function may be written in the form

$$\tilde{U}^{(\mathrm{HS}-)}(\bar{\boldsymbol{\sigma}})=\sum_{r=1}^{n-1}c^{(r)}\psi^{(r)}(\hat{\tau}_{\mathrm{e}}^{(r)})+c^{(n)}\psi^{(n)}(\hat{\tau}_{\mathrm{e}}^{(n)}), \tag{B12}$$

where $\hat{\tau}_{\mathrm{e}}^{(r)}=\sqrt{\bar{\tau}^2(\hat{\omega}^{(r)})^2+\bar{\tau}_{\mathrm{d}}^2(\hat{\eta}^{(r)})^2}$ $(r=1,\ldots,n-1)$ and $\hat{\tau}_{\mathrm{e}}^{(n)}=\tau_{\mathrm{e}}^{(n)}(\hat{\omega}^{(r)},\hat{\eta}^{(r)})$ [as given by (B10)]. The corresponding estimate for the efective stress–strain relation of the incompressible fiber composite then becomes

$$\begin{aligned}\bar{\varepsilon}=&\sum_{r=1}^{n-1}\frac{c^{(r)}}{\hat{\tau}_{\mathrm{e}}^{(r)}}(\psi^{(r)})'(\hat{\tau}^{(r)})\left[(\hat{\omega}^{(r)})^2\bar{\tau}\frac{\partial\bar{\tau}}{\partial\bar{\boldsymbol{\sigma}}}+(\hat{\eta}^{(r)})^2\bar{\tau}_{\mathrm{d}}\frac{\partial\bar{\tau}_{\mathrm{d}}}{\partial\bar{\boldsymbol{\sigma}}}\right]+\cdots\\&+\frac{c^{(n)}}{\hat{\tau}_{\mathrm{e}}^{(n)}}(\psi^{(n)})'(\hat{\tau}_{\mathrm{e}}^{(n)})\left[\left[1+2\left(\frac{1}{c^{(n)}}-\sum_{t=1}^{n-1}\frac{c^{(t)}}{c^{(n)}}\hat{\omega}^{(t)}\right)^2-\sum_{t=1}^{n}\frac{c^{(t)}}{c^{(n)}}(1-(\hat{\omega}^{(t)})^2)\right]\bar{\tau}\frac{\partial\bar{\tau}}{\partial\bar{\boldsymbol{\sigma}}}+\cdots\right.\\&\left.+\left(\frac{1}{c^{(n)}}-\sum_{t=1}^{n-1}\frac{c^{(t)}}{c^{(n)}}\hat{\eta}^{(t)}\right)^2\bar{\tau}_{\mathrm{d}}\frac{\partial\bar{\tau}_{\mathrm{d}}}{\partial\bar{\boldsymbol{\sigma}}}\right]+\cdots\\&+\sum_{r=1}^{n-1}c^{(r)}\bar{\tau}^2\frac{\partial\hat{\omega}^{(r)}}{\partial\bar{\boldsymbol{\sigma}}}\left[\frac{1}{\hat{\tau}_{\mathrm{e}}^{(r)}}(\psi^{(r)})'(\hat{\tau}_{\mathrm{e}}^{(r)})\hat{\omega}^{(r)}+\frac{1}{\hat{\tau}_{\mathrm{e}}^{(n)}}(\psi^{(n)})'(\hat{\tau}_{\mathrm{e}}^{(n)})\left[\hat{\omega}^{(n)}-\frac{2}{c^{(n)}}\left(1-\sum_{t=1}^{n-1}c^{(t)}\hat{\omega}^{(t)}\right)\right]\right]+\cdots\\&+\sum_{r=1}^{n-1}c^{(r)}\bar{\tau}_{\mathrm{d}}^2\frac{\partial\hat{\eta}^{(r)}}{\partial\bar{\boldsymbol{\sigma}}}\left[\frac{1}{\hat{\tau}_{\mathrm{e}}^{(r)}}(\psi^{(r)})'(\hat{\tau}_{\mathrm{e}}^{(r)})\hat{\eta}^{(r)}+\frac{1}{c^{(n)}\hat{\tau}_{\mathrm{e}}^{(n)}}(\psi^{(n)})'(\hat{\tau}_{\mathrm{e}}^{(n)})\left(1-\sum_{t=1}^{n-1}c^{(t)}\hat{\eta}^{(t)}\right)\right].\end{aligned} \tag{B13}$$

We note that each of the terms in the last two sums in (B13) is identical to zero by virtue of the optimization conditions (B11). Thus, in the computation of the effective stress–strain relations, we may regard the optimization variables as constants (as far as derivatives with respect to $\bar{\boldsymbol{\sigma}}$ are concerned). The final result is given by relation (32), where $\hat{\omega}^{(n)}$ and $\hat{\boldsymbol{\eta}}^{(n)}$ are defined via relations (B8) in terms of the $\hat{\omega}^{(r)}$ and $\hat{\boldsymbol{\eta}}^{(r)}$ $(r = 1, \ldots, n-1)$, respectively.

The corresponding expressions for the upper estimates for the effective stress–strain relations of the incompressible fiber composite are computed similarly. It can also be shown that analogous results may be obtained for the *compressible* nonlinear fiber composites.

APPENDIX C: A USEFUL IDENTITY

In many applications, expressions for the effective elasticity tensors of linear-elastic composites involve the evaluation of a fourth-order tensor $\hat{\mathbf{M}}$, defined by

$$\hat{\mathbf{M}} = \left[\sum_{r=1}^{n} c^{(r)} [\mathbf{M}^{(r)}]^{-1} \right]^{-1}, \tag{C1}$$

where $\mathbf{M}^{(r)}$ are positive definite, satisfying the conditions $M^{(r)}_{ijkl} = M^{(r)}_{jikl} = M^{(r)}_{ijlk} = M^{(r)}_{klij}$, and where $\sum_{r=1}^{n} c^{(r)} = 1$ with $0 \leqslant c^{(r)} \leqslant 1$ [see, for example, Hill (1965) and Walpole (1969)]. For later reference, we note that all the symmetries of the tensors $\mathbf{M}^{(r)}$ are carried over to the tensor $\hat{\mathbf{M}}$.

The aim of this appendix is to demonstrate the following identity, which is used repeatedly in the body of the paper:

$$\sigma_{ij} \hat{M}_{ijst} \sigma_{st} = \min_{\boldsymbol{\Omega}^{(r)}, \bar{\boldsymbol{\Omega}} = \mathbf{I}} \left\{ \sum_{r=1}^{n} c^{(r)} \sigma_{ij} \Omega^{(r)}_{klij} M^{(r)}_{klpq} \Omega^{(r)}_{pqst} \sigma_{st} \right\}, \tag{C2}$$

for all second-order symmetric tensors $\boldsymbol{\sigma}$, where the variables $\boldsymbol{\Omega}^{(r)}$ $(r = 1, \ldots, n)$, are subject to the optimization constraint $\sum_{r=1}^{n} c^{(r)} \boldsymbol{\Omega}^{(r)} = \mathbf{I}$, and satisfy the symmetry conditions $\Omega_{ijkl} = \Omega_{jikl} = \Omega_{ijlk}$. This identity is a generalization of an analogous identity, first presented in deBotton and Ponte Castañeda (1992).

We begin by letting $\mathbf{G}(\boldsymbol{\Omega}^{(r)})$ be the function defined by

$$G_{ijst}(\boldsymbol{\Omega}^{(r)}) = \sum_{r=1}^{n} c^{(r)} \Omega^{(r)}_{klij} M^{(r)}_{klpq} \Omega^{(r)}_{pqst}, \tag{C3}$$

where the variables $\boldsymbol{\Omega}^{(r)}$ are subject to the constraint $\bar{\boldsymbol{\Omega}} = \mathbf{I}$, and where the tensors $\mathbf{M}^{(r)}$ and the constants $c^{(r)}$ are as given above. The choice of the set

$$\Omega^{(r)}_{ijkl} = (M^{(r)})^{-1}_{ijpq} \hat{M}_{pqkl}, \tag{C4}$$

satisfies both the optimization constraints and the symmetry conditions stated in (C2), and is such that $\mathbf{G}(\boldsymbol{\Omega}^{(r)}) = \hat{\mathbf{M}}$. We consider next a second, arbitrary set, distinct from the first set, $\hat{\boldsymbol{\Omega}}^{(r)}$ $(r = 1, \ldots, n)$, such that $\bar{\hat{\boldsymbol{\Omega}}}^{(r)} = \mathbf{I}$, and we let $\boldsymbol{\Theta}^{(r)} = \hat{\boldsymbol{\Omega}}^{(r)} - \boldsymbol{\Omega}^{(r)} \neq \mathbf{0}$. Then, substitution of this second set into (C3) leads to

$$\begin{aligned} G_{ijst}(\hat{\boldsymbol{\Omega}}^{(r)}) &= \sum_{r=1}^{n} c^{(r)} (\Omega^{(r)}_{klij} + \Theta^{(r)}_{klij}) M^{(r)}_{klpq} (\Omega^{(r)}_{pqst} + \Theta^{(r)}_{pqst}) \\ &= \sum_{r=1}^{n} c^{(r)} \Omega^{(r)}_{klij} M^{(r)}_{klpq} \Omega^{(r)}_{pqst} + \sum_{r=1}^{n} c^{(r)} \Theta^{(r)}_{klij} M^{(r)}_{klpq} \Theta^{(r)}_{pqst}, \end{aligned} \tag{C5}$$

where we have used the fact that $\bar{\boldsymbol{\Theta}} = \mathbf{0}$. In addition, since the tensors $\mathbf{M}^{(r)}$ are positive definite, it follows that for all nonzero, second order, symmetric tensors $\boldsymbol{\sigma}$,

$$\sigma_{ij} \Theta^{(r)}_{klij} M^{(r)}_{klpq} \Theta^{(r)}_{pqst} \sigma_{st} = (\Theta^{(r)}_{klij} \sigma_{ij}) M^{(r)}_{klpq} (\Theta^{(r)}_{pqst} \sigma_{st}) > 0. \tag{C6}$$

The identity (C2) then follows from (C5) and (C6), because

$$\sigma_{ij} G_{ijkl}(\hat{\boldsymbol{\Omega}}^{(r)}) \sigma_{kl} > \sigma_{ij} G_{ijkl}(\boldsymbol{\Omega}^{(r)}) \sigma_{kl} = \sigma_{ij} \hat{M}_{ijkl} \sigma_{kl}, \tag{C7}$$

for all possible $\hat{\boldsymbol{\Omega}}^{(r)} \neq \boldsymbol{\Omega}^{(r)}$ satisfying the optimization constraint and the symmetry conditions, and nonzero, second order, symmetric tensors $\boldsymbol{\sigma}$.

Finally, we note that this identity can be further generalized to the case of a tensor $\mathbf{M}$ with arbitrary dependence on the position vector $\mathbf{x}$. In this case the summations in (C1) and (C2) are replaced by integrations over the volume Ω. The optimization variables $\boldsymbol{\Omega} = \boldsymbol{\Omega}(\mathbf{x})$ satisfy the symmetry conditions stated in (C2) and the optimization constraint $\int_{\Omega} \boldsymbol{\Omega}(\mathbf{x})\, dx = \mathbf{I}$.